Control Engineering Practice 174 (2026) 107033

Contents lists available at ScienceDirect

Control Engineering Practice

journal homepage: www.elsevier.com/locate/conengprac

Predictive adaptive reactivity-controlled compression ignition for a dual-fuel marine engine: A model-in-the-loop study

Xiaoguo Storm [a], Amir-Mohammad Shamekhi [a], Mohammad Raisi Esfarjani [a,*], Amin Modabberian [b], Aneesh Vasudev [a], Kai Zenger [b], Jari Hyvönen [c], Maciej Mikulski [a,*]

[a] School of Technology and Innovation, Efficient Powertrain Solutions (EPS), University of Vaasa, Wolffintie 34, FI-65200, Vaasa, Finland
[b] School of Electrical Engineering, Aalto University, Maarintie 8, FI-00076, Espoo, Finland
[c] Wärtsilä Finland Oy, Teollisuuskatu 1, 65170, Vaasa, Finland

ARTICLE INFO

Keywords:
Low-temperature combustion
RCCI
Adaptive model predictive control
Real-time model

ABSTRACT

Low-temperature, reactivity-controlled compression ignition (RCCI) combustion has proven instrumental in resolving the long-standing trade-off between engine emissions and efficiency, particularly for heavy-duty applications. However, RCCI has an inherent sensitivity to variations in-cylinder charge composition, such as fuel stratification, temperature gradients, and air-fuel mixing. This makes combustion behavior unpredictable and difficult to regulate using conventional control methods. This study presents an advanced multivariable model-based control design (MBCD) toolchain tailored for marine RCCI engines. Specifically, it introduces a real-time adaptive model predictive control (AMPC) strategy to regulate the indicated mean effective pressure ($IMEP$) and the crank angle at 50% mass fraction burned ($CA50$) by manipulating the total fuel energy and the blend ratio (BR) between the two fuels. The control framework is evaluated through model-in-the-loop (MiL) simulations with an experimentally validated high-fidelity UVATZ (University of Vaasa Advanced Thermo-Kinetic Multi-zone) model of a Wärtsilä 31DF engine combustor as the plant, and a physics-based linear real-time model (RTM) as an observer. The controller's performance is benchmarked against a decentralized PI controller under various transient scenarios. Both controllers achieve comparable tracking of $IMEP$ and $CA50$, but the AMPC demonstrates faster $IMEP$ response (within eight cycles), lower $CA50$ steady-state error (maximum 0.45 crank-angle degree (CAD)), and reduced fuel consumption (2.7%). Additionally, AMPC's receding-horizon framework and self-tuning features enhance robustness against unstructured uncertainties and parameter variations, marking a significant advancement over previously proposed predictive control strategies.

1. Introduction

Low-temperature combustion (LTC) concepts have attracted significant research interest in recent years due to their potential for substantial reduction in emissions, improvements in thermal efficiency, and compatibility with a wide range of fuels. Among LTC strategies, dual-fuel (DF) reactivity-controlled compression ignition (RCCI) has emerged as a promising approach, offering brake thermal efficiencies exceeding 50%, together with ultra-low emissions of nitrogen oxides (NO_x) and soot. These advantages have been demonstrated–albeit at a low technology readiness level–for various low- and zero-carbon fuel combinations, including methanol (Li et al., 2013), ammonia (Fakhari et al., 2023), and hydrogen (Fakhari et al., 2024). Hydrogen, in particular, is a compelling option due to its ability to be blended into natural gas pipelines at concentrations of up to 25% by volume, leveraging existing onboard storage and injection infrastructure (Vasudev et al., 2023). A recent study by Lehtoranta et al. (2023) validated these benefits through real-world sea trials using an RCCI-adapted Wärtsilä 8V31 DF marine engine. The trials further demonstrated that RCCI operation with diesel and natural gas can reduce methane slip by up to 50% compared with the best-performing gas engines currently on the market, signaling a transformative potential for marine propulsion systems.

Despite its advantages, the kinetically driven auto-ignition mechanism of RCCI presents significant challenges for achieving stable and robust operation. RCCI's highly nonlinear behavior can lead to pronounced cycle-to-cycle variations and instability during transient conditions (Duraisamy et al., 2019; Saxena et al., 2022). Additionally, insufficient mixture reactivity at low loads can result in poor combustion

* Corresponding authors.
E-mail addresses: mohammad.raisi.esfarjani@uwasa.fi (M.R. Esfarjani), maciej.mikulski@uwasa.fi (M. Mikulski).

https://doi.org/10.1016/j.conengprac.2026.107033
Received 28 October 2025; Received in revised form 25 February 2026; Accepted 27 April 2026
Available online 5 May 2026

Nomenclature

MBCD	Model-Based Control Design
RCCI	Reactivity-Controlled Compression Ignition
LTC	Low-Temperature Combustion
DF	Dual-Fuel
DI	Direct Injection
AMPC	Adaptive Model Predictive Control
MPC	Model Predictive Control
PI	Proportional-Integral
PID	Proportional-Integral-Derivative
MIMO	Multi-Input Multi-Output
SISO	Single-Input Single-Output
LPV	Linear Parameter-Varying
RTM	Real-Time Model
UVATZ	University of Vaasa Advanced Thermo-Kinetic Multi-Zone model
MiL	Model-in-the-Loop
EiL	Engine-in-the-Loop
RCP	Rapid Control Prototyping
NO_x	Nitrogen Oxides
CFD	Computational Fluid Dynamics
MZM	Multi-Zone Model
SCRE	Single-Cylinder Research Engine
$IMEP$	Indicated Mean Effective Pressure [bar]
$CA50$	Crank angle at 50% mass fraction burned [CAD]
BR	Blend ratio (energy-based) [-]
E_{fuel}	Total fuel energy input [J]
P_{cyl}	In-cylinder pressure
CHR	Cumulative heat release
J	MPC cost function
x_k	State vector at step k
u_k	Control input vector
y_k	Output vector
Δu_k	Control input increment
ΔU	Stacked control input increments
Y	Predicted output vector
$\hat{Y}$	Predicted output vector (model-based prediction)
Y_{ref}	Reference trajectory
$u_{\min}$	Minimum control input constraint
$u_{\max}$	Maximum control input constraint
$y_{\min}$	Minimum output constraint
$y_{\max}$	Maximum output constraint
A, B, C, D	State-space matrices
Q	Output weighting matrix
R	Input weighting matrix
F_k	State-to-output prediction matrix
Φ_k	Toeplitz prediction matrix
D_1, D_2	Disturbance coefficients in state-space model
N_p	Prediction horizon
N_c	Control horizon
T_{int}	Intake temperature [K]
M_{EGR}	EGR mass flow rate
α, β	Model parameters for CA50 dynamics
$\dot{Q}$	Heat transfer rate
$\dot{m}$	Mass flow rate
λ	Air–fuel ratio
λ_{global}	Global in-cylinder air–fuel ratio
D	Mass diffusion coefficient
Λ	Thermal conductivity
A	Flow area
R	Cylinder radius
ζ_t	Mixing intensity factor
ζ_∇	Slope of air–fuel ratio distribution profile
ζ_λ	Air–fuel ratio at the outermost zone
$\Delta Y_i/\Delta w$	Species concentration gradient between zones
$\Delta T/\Delta w$	Temperature gradient between zones
Δw	Distance between neighboring zones
HRF	High-Reactivity Fuel
LRF	Low-Reactivity Fuel
SOI	Start Of Injection
MAE	Mean Absolute Error
RMS	Root Mean Square Error
MPRR	Maximum Pressure Rise Rate
COV	Coefficient of Variation
PPRR	Peak Pressure Rise Rate
PR	Premixed Ratio
CAD	Crank-Angle Degree

efficiency (Mikulski et al., 2018; Mikulski & Bekdemir, 2017; Mikulski et al., 2019), while excessive peak cylinder pressures and pressure rise rates can constrain RCCI operation at high loads (Basina, 2019; Basina et al., 2020). These limitations underscore the need for advanced control strategies which are fast, predictive, and capable of managing multiple parameters simultaneously.

Model-based control offers an effective approach for achieving both optimal engine performance and reduced calibration efforts, particularly in highly complex, nonlinear systems (Paykani et al., 2021). Several model-based control strategies have been proposed for RCCI engines across both light-duty and heavy-duty applications. For instance, Sadabadi et al. developed a physics-based, in-cycle control-oriented model (COM) tailored for RCCI control (Sadabadi, 2015). This model was subsequently simplified and linearized to facilitate the design of a linear quadratic integral (LQI) controller (Khodadadi Sadabadi et al., 2016). The control objective was to regulate combustion phasing, specifically the crank angle at 50% heat release (CA50), by adjusting the energy-based blend ratio (BR) between low-reactivity and high-reactivity fuels (LRF/HRF). The LQI controller demonstrated promising performance, achieving approximately 0.4 crank-angle degree (CAD) of overshoot, zero steady-state error, and a settling time of six engine cycles (Sadabadi & Shahbakhti, 2016).

Building on similar objectives, Kondipati et al. (2017) developed an RCCI combustion phasing controller, targeting CA50 by simultaneously varying the BR and the start of injection (SOI) of HRF. While BR influences the global mixture reactivity, direct injection of HRF via SOI introduces a spatial reactivity gradient within the combustion chamber. A combined feedforward and proportional-integral (PI) feedback controller was implemented and experimentally validated. This achieved a tracking error of approximately 2 CAD and a settling time of three to four engine cycles. However, the controller's single-input, single-output (SISO) structure limited its ability to capture the full dynamics of RCCI operation across a wide range of conditions, and it lacked optimality in control performance. Raut et al. (2018) addressed these limitations with a model predictive control (MPC) strategy based on a hybrid physics-based and empirical COM for RCCI. Their controller simultaneously regulated indicated mean effective pressure ($IMEP$) and $CA50$ by adjusting fuel quantity, BR and SOI timing. By incorporating switched MPC and sensitivity-based selection between SOI and BR, the controller outperformed a conventional proportional-integral-derivative (PID) controller, achieving tracking errors of 1.4 CAD for $CA50$ and 0.26 bar for $IMEP$ in experimental tests.

Data-driven modeling approaches for RCCI combustion are increasingly associated with machine learning techniques (Batool et al., 2023,

2021). Irdmousa et al. (2019) proposed a state-space model (SSM) based on a least-squares support vector machine (LS-SVM) within a linear parameter-varying (LPV) framework. This model was used to develop an MPC for $CA50$, achieving a tracking error of less than 1 CAD. However, the study's experimental validation was conducted under constrained conditions, with key variables such as intake temperature, engine speed, and premixed ratio (PR) manually held constant within a narrow operating range. This limited the assessment of the controller's robustness and adaptability under more realistic, dynamic engine conditions. Moreover, the control strategy primarily focused on single-input (SOI) adjustment, without fully demonstrating the controller's capability to coordinate multiple actuators or manage the complex multivariable interactions characteristic of RCCI combustion.

Subsequent work by the same group extended the MPC framework to include simultaneous control of $IMEP$ and $CA50$, while incorporating a constraint on the maximum pressure rise rate (MPRR) (Basina et al., 2020). Additional contributions included the use of kernelized canonical correction analysis (KCCA) for optimal state identification in LPV models (Irdmousa et al., 2021), and modeling of fuel stratification dynamics (Irdmousa et al., 2023).

GhafGhanbari et al. (2024) introduced Bayesian neural networks (BNNs) to capture stochastic uncertainties in the states and inputs of the SSM. A scenario-based MPC was simulated, demonstrating strong tracking performance. However, the complexity of the methodology and the increased computational burden relative to standard MPC approaches raise concerns about its feasibility for real-time implementation. Furthermore, the trade-off between tracking accuracy and constraint satisfaction remains a critical consideration for practical deployment.

In another study, Irdmousa et al. (2023) focused on controlling combustion cyclic variability (COV_{IMEP}) to keep it below 3% using a nonlinear MPC framework based on physics-informed models of $CA50$ and $IMEP$. Their research progressed toward linearizing a physics-based control-oriented model into a constant state-space LPV form for MPC implementation (Batool et al., 2023). However, the controller was validated only for BR ranging from 0% to 50%, which is not representative of typical RCCI operation. In practice, RCCI engines operate at significantly higher BRs, especially under high-load conditions, to fully exploit the benefits of reduced emissions.

To address both air-path and fuel-path dynamics, Verhaegh et al. (2022) developed an uncertainty model to account for cylinder-to-cylinder variations. They experimentally validated a multivariable PID feedback controller with inputs including low- and high-reactivity fuel energies, diesel SOI, variable geometry turbine (VGT) position, and exhaust gas recirculation (EGR) valve position. Using a frequency-domain approach, the multi-input multi-output (MIMO) controller demonstrated effective tracking of $IMEP$, $CA50$, EGR ratio, exhaust manifold pressure and BR during transient conditions. Notably, the controller was capable of mitigating disturbances in intake temperature caused by inter-cylinder variability.

Following this, Vlaswinkel and Willems (2024) employed principal component decomposition (PCD) and Gaussian process regression to reconstruct in-cylinder pressure traces and key combustion metrics - $IMEP$, $CA50$, and peak pressure rise rate (PPRR) - along with their cycle-to-cycle variations. While the method showed promise for in-cylinder pressure shaping and combustion optimization, relatively high absolute prediction errors may hinder its applicability in advanced control development (Vlaswinkel & Willems, 2023).

Fast computation and high prediction accuracy are fundamental requirements for effective MPC. However, achieving both simultaneously remains a challenge in existing RCCI control frameworks. Our previous work (Storm et al., 2023) introduced and validated a physics-based, cycle-to-cycle real-time model (RTM) to address the demands of highly nonlinear RCCI engine dynamics. This model was rigorously benchmarked against the University of Vaasa Advanced Thermo-Kinetic Multi-Zone (UVATZ) model (Storm et al., 2023; Vasudev et al., 2022a,b), which served as the reference for its development.

The RTM provides not only cycle-averaged combustion metrics but also crank-angle-resolved cylinder pressure and heat release profiles. It achieves fast in-cycle simulation times while maintaining accuracy across a wide operating range, including transient conditions. A detailed description of the RTM methodology, governing equations, and validation scenarios are provided in (Storm et al., 2023). This model represents a significant advance over earlier, more simplistic RCCI combustion models by effectively balancing model fidelity and computational efficiency. This was made possible through its LPV structure, which enables real-time applicability without compromising predictive performance.

The RTM provides a solid foundation for model-based control, but the current state of MPC for RCCI engines still faces significant challenges, particularly in handling large parameter variations, actuator coordination, and highly nonlinear system dynamics. These challenges are compounded by the fact that most existing MPC implementations rely on fixed or simplified models, which limit their ability to adapt to dynamic engine behavior and maintain optimal performance across varying conditions. In other words, conventional MPC approaches relying on fixed models often fail to maintain control performance across varying operating conditions and transient events. This highlights the need for adaptive model predictive control (AMPC) strategies, wherein the controller dynamically updates its internal model at each operating point and during each optimization cycle. Such adaptability enables more robust and accurate control of RCCI combustion, ensuring consistent performance across a broad range of engine conditions.

Punasiya and Sarangi (2024) developed an LPV state-space model using a data-driven approach and integrated it into an AMPC framework for tracking $CA50$ and $IMEP$, while accounting for MPRR constraints. Although the model-in-the-loop (MiL) simulations demonstrated a maximum absolute tracking error of 9.7%, the controller's performance was constrained by the dispersion and sparsity of the training data, limiting its generalizability across broader operating conditions.

The main contributions of this study are summarized as follows:

- **Adaptive model predictive control:** A real-time AMPC scheme is formulated to regulate $IMEP$ and $CA50$ via total fuel energy and blend ratio in a dual-fuel marine RCCI engine.
- **Observer-based LPV modeling:** A novel linear parameter-varying RTM is embedded as an observer within the AMPC loop, enabling cycle-by-cycle model updates that capture coupling and nonlinearity while remaining computationally feasible.
- **High-fidelity MiL validation:** The AMPC is evaluated through MiL simulations using the high-fidelity multi-zone UVATZ model (Vasudev et al., 2022a) of a Wärtsilä 31DF marine engine combustor, which poses substantial challenges due to its sensitivity and detailed representation of multi-zone thermodynamic and chemical-kinetic phenomena.
- **Benchmarking against decentralized PI:** Despite the complexity of the UVATZ plant, the AMPC achieves faster $IMEP$ response (within eight cycles), lower $CA50$ steady-state error (maximum 0.45 CAD), and reduced fuel consumption (2.7%) compared with a decentralized PI benchmark.
- **Robustness and constraint handling:** The receding-horizon formulation and self-tuning updates enhance robustness to unstructured uncertainties (e.g., intake/EGR disturbances) and allow explicit enforcement of input-rate and output constraints, which are difficult to guarantee with PI.
- **End-to-end toolchain:** To the best of the authors' knowledge, this work, alongside our previous contribution (Modabberian et al., 2024), represents one of the first comprehensive efforts in adaptive MPC design for marine RCCI engines, offering a significant advance over previously proposed predictive control strategies.

Section 2 presents the modeling framework for RCCI control, introducing the high-fidelity UVATZ plant model and the linearized RTM used for the predictive control, along with its validation. Section 3 de-

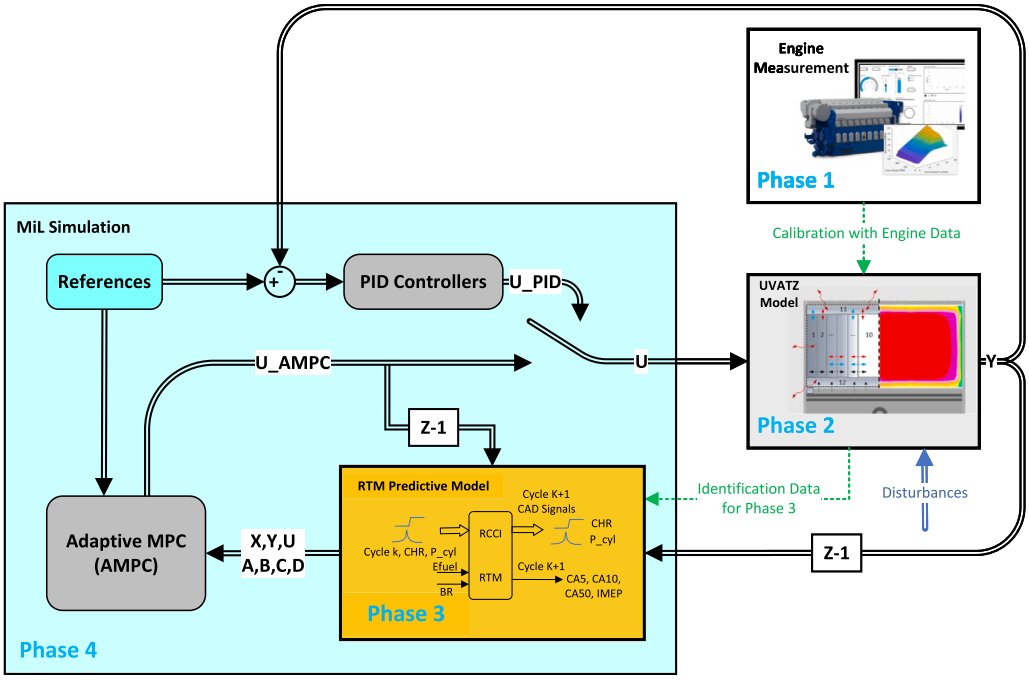

Fig. 1. Model-based control design workflow diagram.

scribes the development of the control strategies, including the baseline PI controller and the AMPC framework, and outlines the test scenarios. Section 4 provides a comprehensive comparative analysis of the controllers by presenting the simulation results, starting with parameter tuning and progressing from baseline validation under ideal conditions to increasingly complex scenarios involving mid-load and high-load transients, disturbances, and actuator constraints. Finally, Section 5 concludes the paper by summarizing the key findings and discussing future research directions.

2. The control object and modeling framework

The workflow of this MiL study comprises four distinct phases, each related to the identification of the control object and the calibration of the models involved. Fig. 1 illustrates the four phases.

Phases 1 and 2 involve the calibration of the physics-based, multi-zone UVATZ model, using initial steady-state RCCI experiments conducted on the Wärtsilä single-cylinder research engine (SCRE W31DF), which serves as the control object. The calibration methodology is detailed in the works of Vasudev et al. (2022a,b), and summarized in Section 2.1 to ensure reproducibility.

The UVATZ model solves detailed chemical kinetics, which is the core mechanism governing RCCI combustion. It also incorporates phenomenological models for in-cylinder flow and heat transfer. This enables it to extrapolate the results across the calibration space with high fidelity. However, this level of detail is at the expense of computational speed, requiring approximately three minutes per simulated combustion cycle.

The workflow leverages the UVATZ model in two key ways to address the scarcity of experimental data. Firstly, 51 additional steady-state and 33 transient operating points were simulated between the two experimentally calibrated references. These simulations generated a comprehensive dataset for training the RTM model developed in Phase 3. The dataset spans a wide range of fuel quantities, blend ratios, and intake mixture conditions at valve closing, thereby covering the full calibration space required by the RTM. Secondly, the calibrated UVATZ model is employed as the plant model for transient MiL simulations in Phase 4. Its high fidelity allows it to capture disturbances as they would occur in a physical combustion system, making it an ideal benchmark for control system evaluation.

Phase 4 is this study's core contribution, where both PI and AMPC strategies are implemented for simultaneous control of $IMEP$ and $CA50$ under identical testing conditions. The RTM (Storm et al., 2023) is used for AMPC design, serving both as the system representation and as the LPV model within the AMPC framework. The designed control system is then tested using the UVATZ model (Vasudev et al., 2022a, 2024, 2022b) as the plant model.

The additional implementation of PI controllers provides a valuable benchmark for assessing the AMPC's performance. Ultimately, both control strategies are compared and analyzed to evaluate their effectiveness in managing RCCI combustion dynamics.

2.1. High-fidelity multi-zone plant model (UVATZ)

The UVATZ model is a physics-based, multi-zone, thermo-kinetic simulation tool developed by Vasudev et al. (2022a, 2024). It serves as the high-fidelity plant model in this study, offering detailed and predictive in-cylinder RCCI combustion dynamics that are essential for validating control strategies. The UVATZ model employs an onion-skin, multi-zone structure, which divides the in-cylinder volume into a series of coaxial zones as shown in Fig. 2. This zonal structure along with individual volumes of each zone has been calibrated (Vasudev et al., 2024) to phenomenologically capture direct injection (DI) pilot fuel stratification, thermal gradients, and wall heat transfer. The zonal structure consists of 12 zones supporting computational efficiency and accuracy (Vasudev et al., 2022a).

The zones, operating as individual homogeneous reactors, are coupled together based on equalized pressure within the multi-zone model (MZM) at any time instant. This assumption alleviates the need for the momentum conservation equation. As a result, the interzonal boundaries move freely according to the thermodynamic state of the neighboring zone, causing work exchange between the zones in the process (black arrows in Fig. 2). Interzonal heat ($\dot{Q}$) and mass ($\dot{m}$) flows are modeled phenomenologically with a 0-dimensional energy-cascade turbulence sub-model resulting in governing differential equations that include mass, chemical species, and energy balances for each zone. Addi-

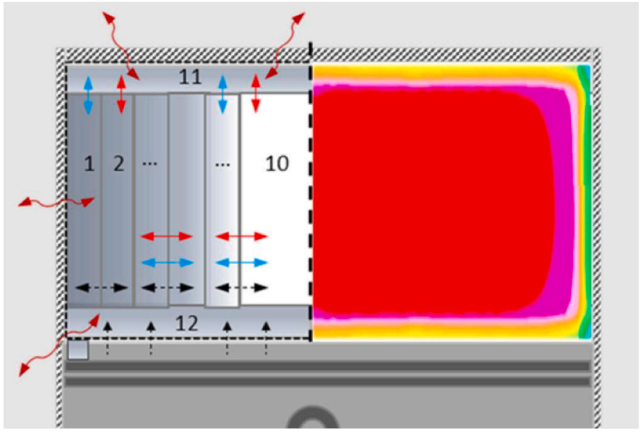

Fig. 2. Generalized multi-zone framework. The zonal configuration of multi-zone model (MZM) (left) is compared to the CFD simulations (right). Heat flow, mass flow, and work are represented with red, blue, and black arrows, respectively (Adapted from Kakoee et al., 2023), with permission from the authors. (For interpretation of the references to colour in this figure legend, the reader is referred to the web version of this article.)

tionally, pressure and temperature of each zone is coupled by the ideal gas equation, and the entire in-cylinder volume is the sum of volume for each individual zone. $\dot{Q}$ and $\dot{m}$ are depicted in Fig. 2 by red and blue arrows, respectively. The flows are modeled based on thermal and composition gradients as presented in Eq. (1):

$$\begin{aligned} {}^{IZT}\dot{m}_{i,z\to z+1} &= \zeta_t \left(\mathfrak{D}\rho A \frac{\Delta Y_i}{\Delta w} \right)_{z\to z+1} \\ {}^{IZT}\dot{Q}_{z\to z+1} &= \zeta_t \left(\Lambda A \frac{\Delta T}{\Delta w} \right)_{z\to z+1} \end{aligned} \tag{1}$$

Here $\Delta Y_i/\Delta w$ and $\Delta T/\Delta w$ are composition and thermal gradients, respectively. Additionally, Δw is the distance between the neighboring zones (z and $z+1$), ζ_t is the mixing intensity factor, A is the flow area, $\mathfrak{D}$ is the mass diffusion coefficient and Λ is the thermal conductivity (Vasudev et al., 2022a). The primary mechanism of heat exchange with the environment (zones #10 to #12) is driven by convection, which is modelled according to the correlation proposed in (Chang et al., 2004). This approach is suitable for the temperature regime and convection-dominant heat transfer in LTC processes. The injection profile of the UVATZ is assumed to be linear in the air-fuel ratio (λ) domain and mapped onto the zones according to Eq. (2)

$$\lambda_{global} = \frac{1}{R}\int_0^R (\zeta_\nabla r + \zeta_\lambda) dr, \tag{2}$$

where λ_{global} is the in-cylinder air-fuel ratio of HRF, R is the cylinder radius, ζ_λ is the λ_{HRF} in the outermost zone and ζ_∇ is the slope of the λ distribution profile. A semi-detailed reaction mechanisms (Yao et al., 2017) involving up to approximately 200 species captures the combustion reactions including NO_x formation. The UVATZ model is implemented in C++ and employs the Cantera libraries (Goodwin et al., 2025) to compute the thermo-kinetic equations. The naturally stiff system is solved with the CVODE solver. Table 1 summarises the modelling choices, with complete details found in the earlier work (Vasudev et al., 2024).

The described level of detail allows the model to accurately simulate the effects of varying BR, which directly influence in-cylinder reactivity distribution and auto-ignition behavior. As these dynamics are resolved both spatially and temporally, UVATZ is well suited for analyzing the impact of control inputs and disturbances on combustion performance. Moreover, the UVATZ model is capable of simulating both internal and external disturbances by accounting for their influence on charge stratification, ignition timing, and heat release characteristics. This makes it an ideal platform for evaluating the robustness of control systems under a wide range of operating conditions.

Table 1
Governing assumptions of UVATZ model (reproduced from Arora and Shahbakhti (2017) with permission of the authors).

Source code	C++ with Cantera libraries (Goodwin et al., 2025)
Gov. assumptions	• Axisymmetric in-cylinder fluid flow • Common zone pressure • Fuel injection decoupled from combustion • Ideal gas
Gov. equations	Mass, energy and species balance; equation of state
Zonal configuration	12 zones (10× annular cylinder; 2× disc zones)
Interzonal heat and mass flow	Temperature and concentration gradient-based; turbulence energy cascade (Bozza et al., 2019)
HRF stratification	Empirical model trained by CFD spray simulations (Vasudev et al., 2024)
Wall heat loss	According to Chang et al. (2004); zone dependent
Reaction mechanism	According to Yao et al. (2017) + NO_x scheme (Sun and Reitz, 2006)
Validation	Wärtsilä 31DF RCCI (Kakoee et al., 2023; Vasudev et al., 2022a)
Solver	CVODE (Cohen et al., 1996), tolerance = 1e-9; max. time step = 2e-6 s

The UVATZ model has been calibrated for the Wärtsilä W31DF research engine setup and validated against experimental data from the Wärtsilä single-cylinder research engine (SCRE W31DF), which operates in RCCI mode using natural gas as LRF and light fuel oil (LFO) as HRF. Table 2 summarizes the engine specifications. The HRF is directly injected into the cylinder via a high-pressure common-rail system, while the LRF is port-injected upstream of the intake valves. Intake air temperature and pressure are regulated using an external air compressor. Comprehensive information on the model formulation, calibration procedure, and validation results can be found in Vasudev et al. (2022a, 2024) and Storm et al. (2023).

2.2. Linearized real-time model for the predictive control

The RTM is a second-order linear, physics-based combustion model developed by Storm et al. (2023). It predicts the crank-angle-resolved in-cylinder pressure and heat release profile of the next combustion cycle using the current cycle's heat release profile and fueling information. The control inputs are the total fuel energy input (E_{fuel}) and the energy-based blend ratio (BR) between gas and diesel fuels.

The RTM is formulated as a linear state-space model, as expressed in Eq. (3). The linearization is computed numerically by approximating the partial derivatives of CHR, P_{cyl} and $IMEP$ with respect to the control inputs at equilibrium points corresponding to mid- and high-load operating conditions.

$$\begin{bmatrix} CHR_{k+1} \\ P_{\text{cyl},k+1} \\ IMEP_{k+1} \end{bmatrix} = \begin{bmatrix} CHR_k \\ P_{\text{cyl},k} \\ IMEP_k \end{bmatrix} + \begin{bmatrix} \frac{\partial CHR}{\partial E_{\text{fuel}}} & \frac{\partial CHR}{\partial BR} \\ \frac{\partial P_{\text{cyl}}}{\partial E_{\text{fuel}}} & \frac{\partial P_{\text{cyl}}}{\partial BR} \\ \frac{\partial IMEP}{\partial E_{\text{fuel}}} & \frac{\partial IMEP}{\partial BR} \end{bmatrix} \tag{3}$$

$$\begin{bmatrix} \Delta E_{\text{fuel},k} \\ \Delta BR_k \end{bmatrix} + \begin{bmatrix} D_{1,CHR_k} & D_{2,CHR_k} \\ D_{1,P_{\text{cyl},k}} & D_{2,P_{\text{cyl},k}} \\ D_{1,IMEP_k} & D_{2,IMEP_k} \end{bmatrix} \begin{bmatrix} T_{\text{int}} \\ M_{\text{EGR}} \end{bmatrix}$$

The partial derivatives in Eq. (3) are defined in Eq. (4).

$$\begin{aligned} &\frac{\partial CHR}{\partial E_{\text{fuel}}} = \frac{CHR}{E_{\text{fuel}}}, \quad \frac{\partial CHR}{\partial BR} = a_1 \cdot CHR, \\ &\frac{\partial P_{\text{cyl}}}{\partial E_{\text{fuel}}} = \frac{dP_{\text{cyl}}}{\Delta E_{\text{fuel}}}, \quad \frac{\partial P_{\text{cyl}}}{\partial BR} = a_2 \cdot dP_{\text{cyl}}, \\ &\frac{\partial IMEP}{\partial E_{\text{fuel}}} = \frac{dIMEP}{\Delta E_{\text{fuel}}}, \quad \frac{\partial IMEP}{\partial BR} = \frac{dIMEP}{dBR} \end{aligned} \tag{4}$$

To account for the influence of intake temperature (T_{int}) and EGR mass flow (M_{EGR}), zero-mean Gaussian process disturbance terms are introduced for each output in Eq. (3), with the detailed applied values discussed in Storm et al. (2023). These disturbances effectively represent additive, unstructured uncertainties of the linear system model.

Given that the state transition matrix (A) is the identity matrix, the states evolve independently. Consequently, the $IMEP$ update equation simplifies to Eq. (5).

$$IMEP_{k+1} = IMEP_k + \begin{bmatrix} \frac{\partial IMEP}{\partial E_{\mathrm{fuel}}} & \frac{\partial IMEP}{\partial BR} \end{bmatrix} \begin{bmatrix} \Delta E_{\mathrm{fuel},k} \\ \Delta BR_k \end{bmatrix} + \begin{bmatrix} D_{1,IMEP_k} & D_{2,IMEP_k} \end{bmatrix} \begin{bmatrix} T_{\mathrm{int}} \\ M_{\mathrm{EGR}} \end{bmatrix} \tag{5}$$

Although the RTM effectively captures $IMEP$ and pressure dynamics, $CA50$ cannot be directly represented in a state-space format due to its indexing-based nature. A data-driven, piecewise constant-parameter model is employed for $CA50$, overcoming this limitation. As a result, the combined model is formulated as Eq. (6).

$$\begin{bmatrix} IMEP_{k+1} \\ CA50_{k+1} \end{bmatrix} = \begin{bmatrix} 1 & 0 \\ 0 & 1 \end{bmatrix} \begin{bmatrix} IMEP_k \\ CA50_k \end{bmatrix} + \begin{bmatrix} \frac{\partial IMEP}{\partial E_{\mathrm{fuel}}} & \frac{\partial IMEP}{\partial BR} \\ \alpha & \beta \end{bmatrix} \begin{bmatrix} \Delta E_{\mathrm{fuel},k} \\ \Delta BR_k \end{bmatrix} + \begin{bmatrix} D_{1,IMEP_k} & D_{2,IMEP_k} \\ D_{1,CA50_k} & D_{2,CA50_k} \end{bmatrix} \begin{bmatrix} T_{\mathrm{int}} \\ M_{\mathrm{EGR}} \end{bmatrix}$$

$$\begin{bmatrix} y_{1k} \\ y_{2k} \end{bmatrix} = \begin{bmatrix} 1 & 0 \\ 0 & 1 \end{bmatrix} \begin{bmatrix} IMEP_k \\ CA50_k \end{bmatrix} \tag{6}$$

The parameters α and β are assumed constant at specific operating points. For instance, at a mid-load operating condition, the model takes the form of Eq. (7).

$$\begin{bmatrix} IMEP_{k+1} \\ CA50_{k+1} \end{bmatrix} = \begin{bmatrix} 1 & 0 \\ 0 & 1 \end{bmatrix} \begin{bmatrix} IMEP_k \\ CA50_k \end{bmatrix} + \begin{bmatrix} \frac{\partial IMEP}{\partial E_{\mathrm{fuel}}} & \frac{\partial IMEP}{\partial BR} \\ -0.00016 & 110.6 \end{bmatrix} \begin{bmatrix} \Delta E_{\mathrm{fuel},k} \\ \Delta BR_k \end{bmatrix} + \begin{bmatrix} D_{1,IMEP_k} & D_{2,IMEP_k} \\ D_{1,CA50_k} & D_{2,CA50_k} \end{bmatrix} \begin{bmatrix} T_{\mathrm{int}} \\ M_{\mathrm{EGR}} \end{bmatrix}$$

$$\begin{bmatrix} y_{1k} \\ y_{2k} \end{bmatrix} = \begin{bmatrix} 1 & 0 \\ 0 & 1 \end{bmatrix} \begin{bmatrix} IMEP_k \\ CA50_k \end{bmatrix} \tag{7}$$

The RTM formulation in Eqs. (3)-(7) includes additive disturbance terms to account for the influence of intake temperature and EGR mass flow. However, these terms are not included in the prediction model used within the AMPC framework in this study, because for the purpose of predictive control, the RTM must be employed in a deterministic form, where the disturbance contributions are neglected and treated as unmodeled dynamics. This simplification reduces computational complexity and ensures numerical tractability of the optimization problem, while maintaining sufficient prediction accuracy. The effect of disturbances is instead captured through the high-fidelity UVATZ model used as the plant in the MiL simulations, allowing the controller's robustness to be evaluated under realistic operating conditions.

Based on the above considerations, the RTM used for prediction in the AMPC framework is expressed in the following deterministic state-space form:

$$\begin{bmatrix} IMEP_{k+1} \\ CA50_{k+1} \end{bmatrix} = \begin{bmatrix} 1 & 0 \\ 0 & 1 \end{bmatrix} \begin{bmatrix} IMEP_k \\ CA50_k \end{bmatrix} + \begin{bmatrix} \frac{\partial IMEP}{\partial E_{\mathrm{fuel}}} & \frac{\partial IMEP}{\partial BR} \\ -0.00016 & 110.6 \end{bmatrix} \begin{bmatrix} \Delta E_{\mathrm{fuel},k} \\ \Delta BR_k \end{bmatrix}$$

$$\begin{bmatrix} y_{1k} \\ y_{2k} \end{bmatrix} = \begin{bmatrix} 1 & 0 \\ 0 & 1 \end{bmatrix} \begin{bmatrix} IMEP_k \\ CA50_k \end{bmatrix} \tag{8}$$

2.3. Validation of the real-time model against UVATZ

Following calibration and full-scale validation, the RTM has been shown to be real-time capable while maintaining high predictive accuracy. It predicts all in-cylinder, pressure-derived combustion indicators within a 7% error margin compared to steady-state experimental data. In transient validation, the root mean square (RMS) errors for $CA5$ and $CA50$ remain below 1.5 CAD, and $IMEP$ is predicted with an absolute error of 0.8 bar. With simulation times under 5 milliseconds per combustion cycle, the RTM is well-suited for the real-time model predictive control of RCCI combustion (Storm et al., 2023).

A step response analysis has been conducted for both the UVATZ and RTM models, further illustrating the latter's dynamic behavior. Step changes are applied to ΔE_{fuel} and ΔBR in the first cycle, with a simulation sampling time of 1 second over three cycles. The results, shown in Fig. 3, compare the $CA50$ and $IMEP$ responses scaled against the initial UVATZ conditions. Both models exhibit consistent trends: a 5% increase in E_{fuel} and a 2% decrease in BR lead to higher $IMEP$ and $CA50$. The mean absolute errors for both outputs remain below the 5% threshold.

These results and prior validation (Storm et al., 2023) confirm that the RTM accurately captures the dynamic behavior of the UVATZ model and is therefore suitable for closed-loop control development.

3. Control strategy development for RCCI engines

RCCI was developed to simultaneously improve engine efficiency and reduce emissions. However, the inherent complexity of reactivity-controlled combustion presents significant challenges for control design. These include high nonlinearities, tight coupling effects between subsystems, and highly dynamic system responses. Optimal control strategies are essential to ensure efficient, stable, and low-emission combustion across the full engine operating range.

This study explores both PI and AMPC strategies as suitable control solutions, implementing and evaluating them under identical testing conditions, as illustrated in Fig. 4. The PI controller is included not only because it is one of the most widely adopted methods in internal combustion engine applications, but also because it serves as a benchmark for assessing the performance of the AMPC approach. Its simplicity, robustness, and ease of implementation make PI a practical and reliable choice, particularly in industrial contexts where computational resources may be limited. By establishing a decentralized PI control structure, the study provides a meaningful reference point for evaluating the added value of predictive and optimization-based control. A comprehensive comparative assessment of established and advanced control strategies, are presented in Appendix 5, further substantiating the selection of PI and adaptive MPC as well-balanced choices in terms of performance, robustness, constraint handling, and implementation complexity.

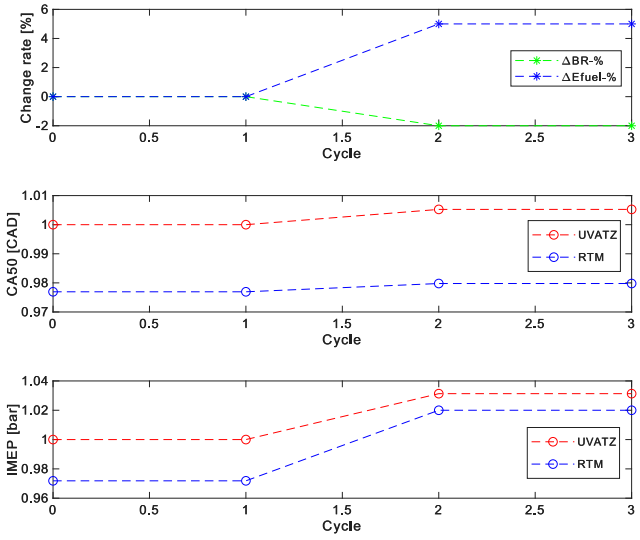

Fig. 3. Step response comparison of the UVATZ and RTM models: $CA50$ and $IMEP$ values are normalized with respect to the initial conditions of the UVATZ model.

The control system was initially designed using the RTM and subsequently tested with both the RTM and the UVATZ models serving as plant models. The RTM-based implementation confirms the system's real-time capability. Control inputs in the PI setup are generated by continuously computing the error between reference and measured values, which are then applied to the UVATZ model. In contrast, the AMPC framework uses the RTM to predict the system's next-cycle behavior based on measurements from the UVATZ model. The RTM provides updated state-space matrices to the AMPC controller, which then solves an optimization problem to determine the optimal control actions. These actions are subsequently applied to the UVATZ model.

The performance of both control strategies is evaluated through closed-loop simulations under various transient conditions. This comparative analysis provides insight into the effectiveness and robustness of each approach in managing RCCI combustion dynamics.

The following subsections present a detailed discussion of each controller, with a particular focus on the formulation and implementation of the AMPC strategy.

3.1. PI control implementation

A decentralized PI control structure is implemented to establish a baseline for comparison with the AMPC controller. A decentralized approach suits the MIMO nature of the RCCI engine system, with individual PI controllers assigned to each input-output pair. Effective decentralized control requires careful input-output pairing to minimize loop interactions. Based on a review of existing engine control literature (Arora & Shahbakhti, 2017; Kondipati et al., 2017; Raut et al., 2018), and the authors' domain expertise, $CA50$ is regulated via the blend ratio (BR), while $IMEP$ is controlled through the total fuel energy input (E_{fuel}).

This configuration provides a practical and well-structured foundation for evaluating the performance of the AMPC strategy under identical operating conditions.[1]

[1] This means that the relative gain array (RGA) is approximately equal (i.e., close) to the identity matrix, confirming low loop interaction and supporting the application of decentralized PI controllers.

3.2. Adaptive model predictive control framework

MPC is a model-based strategy that optimizes control actions over a finite prediction horizon using a dynamic model of the plant. At each control interval, the controller predicts future outputs, minimizes a cost function, and applies the first element of the optimal control sequence. This receding-horizon approach enables MPC to handle multivariable interactions, input-output constraints, and strong loop couplings more effectively than decentralized controllers.

This work models the RCCI combustion engine as an LPV system, whose dynamics change with operating conditions. The RTM prediction model defined in Eq. (8) provides updated linearized state-space matrices (A_k, B_k, C_k, D_k) at each engine cycle, allowing the adaptive MPC (AMPC) to continuously refresh its prediction model. This configuration effectively forms a model predictive self-tuning regulator (MP-STR) that can adapt to real-time plant behavior.

The prediction model is expressed in the discrete-time state-space form shown in Eq. (9).

$$\begin{aligned} x_{k+1} &= A_k\, x_k + B_k\, u_k \\ y_k &= C_k\, x_k + D_k\, u_k \end{aligned} \tag{9}$$

Where $x_k \in \mathbb{R}^n$ is the state vector, $u_k \in \mathbb{R}^m$ the manipulated inputs ($u_k = [\Delta E_{fuel,k}, \Delta BR_k]^T$), and $y_k \in \mathbb{R}^p$ the controlled outputs ($y_k = [IMEP_k, CA50_k]^T$). To facilitate constraint handling and suppress aggressive input moves, the optimization is formulated in incremental form, with input increments defined in Eq. (10).

$$\Delta u_k \equiv u_k - u_{k-1} \tag{10}$$

Over a control horizon of length $N_c \in \mathbb{N}$, the decision vector stacks the future input increments as $\Delta U \in \mathbb{R}^{mN_c}$. Using the standard prediction formulation built from (A_k,B_k,C_k,D_k), the stacked output predictions over a prediction horizon $N_p \in \mathbb{N}$ are written as in Eq. (11).

$$\begin{aligned} \hat{Y} &= F_k\, x_k + \Phi_k\, \Delta U \\ F_k &= \begin{bmatrix} C_k A_k \\ C_k A_k^2 \\ \vdots \\ C_k A_k^{N_p} \end{bmatrix}, \\ \Phi_k &= \begin{bmatrix} C_k B_k & 0 & 0 & \cdots & 0 \\ C_k A_k B_k & C_k B_k & 0 & \cdots & 0 \\ C_k A_k^2 B_k & C_k A_k B_k & C_k B_k & \cdots & 0 \\ \vdots & \vdots & \vdots & \ddots & \vdots \\ C_k A_k^{N_p-1} B_k & C_k A_k^{N_p-2} B_k & C_k A_k^{N_p-3} B_k & \cdots & C_k A_k^{N_p-N_c} B_k \end{bmatrix} \end{aligned} \tag{11}$$

Where $\hat{Y} \in \mathbb{R}^{pN_p}$ collects ($\hat{y}_{k+1}$,$\hat{y}_{k+2}$,$\cdots$,$\hat{y}_{k+N_p}$), $F_k \in \mathbb{R}^{pN_p \times n}$ is the state-to-output prediction matrix, and $\Phi_k \in \mathbb{R}^{pN_p \times mN_c}$ is the Toeplitz matrix that maps input increments to future outputs. This compact representation avoids recursive unrolling and directly connects ΔU to future outputs.

The control objective is defined by the quadratic cost function in Eq. (12).

$$J(\Delta U) = (Y_{\text{ref}} - \hat{Y})^{\mathrm{T}}\, Q\, (Y_{\text{ref}} - \hat{Y}) + \Delta U^{\mathrm{T}}\, R\, \Delta U \tag{12}$$

Where $Y_{ref} \in \mathbb{R}^{pN_p}$ stacks the reference trajectory for $IMEP$ and $CA50$ across the horizon N_p, $Q \in \mathbb{R}^{pN_p \times pN_p}$ is a positive semidefinite output-weighting matrix, and $R \in \mathbb{R}^{mN_c \times mN_c}$ is a positive definite move-suppression matrix. The resulting optimization problem, shown in Eq. (13), is a convex quadratic program that is solved at each sampling instant.

$$\begin{aligned} \min_{\Delta U} \quad & J(\Delta U) \\ \text{s.t.} \quad & \Delta u^{\min} \le \Delta u(k+i) \le \Delta u^{\max}, \quad i = 1, \ldots, N_c \\ & y^{\min} \le \hat{y}(k+i) \le y^{\max}, \quad i = 1, \ldots, N_p \end{aligned} \tag{13}$$

In the optimization problem, the $\Delta u^{\min}, \Delta u^{\max} \in \mathbb{R}^m$ impose bounds on the input increments (e.g., actuator rate limits) and $y^{\min}$, $y^{\max} \in \mathbb{R}^p$

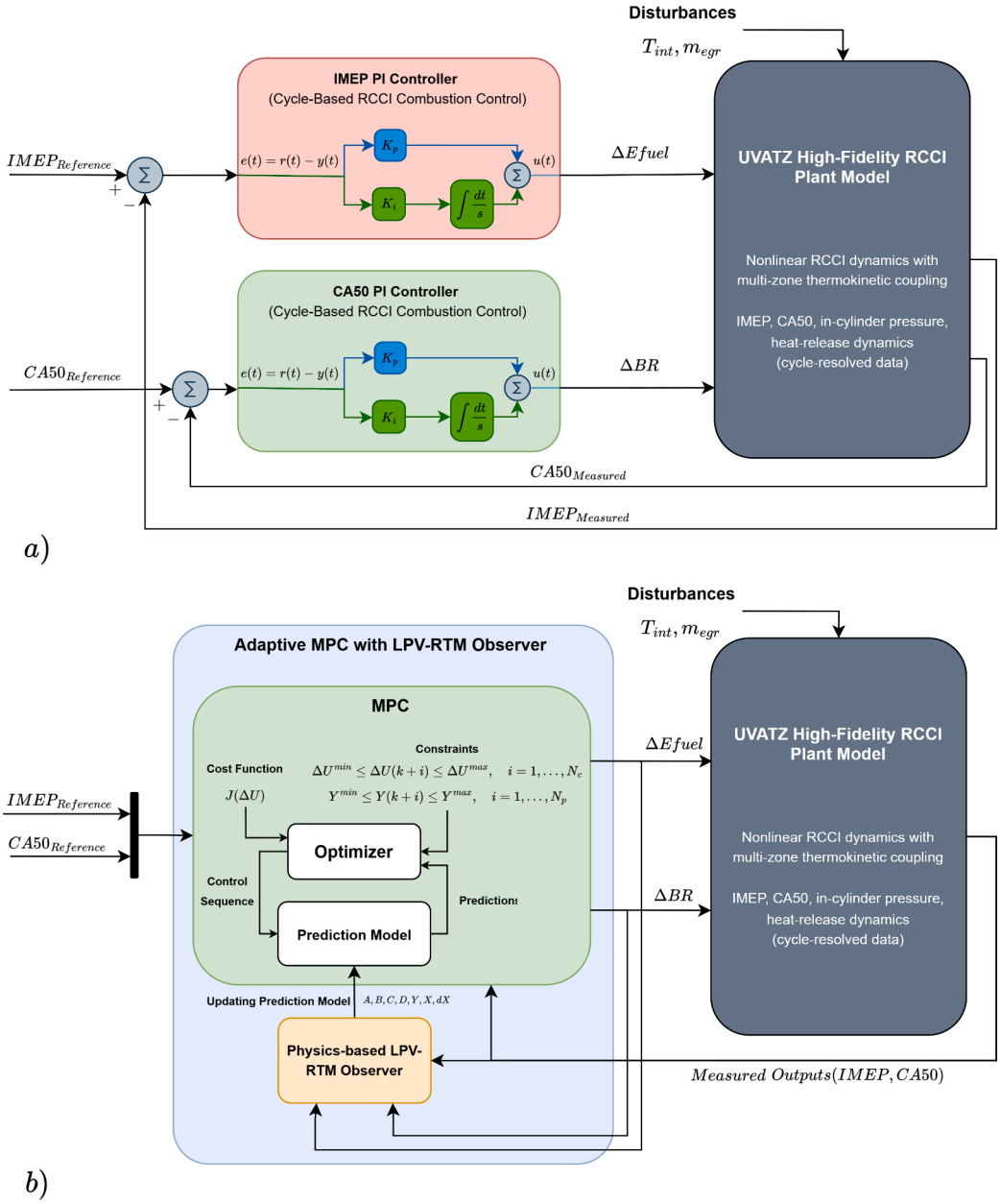

Fig. 4. Closed-loop control architectures investigated in this study: (a) decentralized PI control and (b) adaptive MPC with the LPV real-time model (RTM) observer, applied to the UVATZ high-fidelity RCCI plant model.

impose bounds on the predicted outputs (e.g., operational or emissions-related constraints). After computing the optimal input sequence, only the first increment is applied, and the actual input is updated according to Eq. (14).

$$u_k = u_{k-1} + \Delta u_k \tag{14}$$

The horizon then shifts forward, and the process repeats with refreshed measurements and an updated model. This closed-loop structure ensures that the predictive model remains synchronized with the current operating condition, enabling accurate tracking of $IMEP$ and $CA50$, while respecting safety and performance constraints.

The AMPC is implemented in a MiL environment using Simulink. The UVATZ engine model provides real-time measurements, which are processed by the RTM to generate updated linearization for the controller. Embedded MATLAB functions (MathWorks, 2023) and custom C code manage data exchange, constraint scheduling, and quadratic programming, ensuring real-time feasibility. This integrated workflow, from the plant measurements to the RTM updates, optimization, and actuator commands, forms the backbone of the adaptive predictive control strategy evaluated in this study.

3.3. Test scenarios and evaluation plan

Table 3 summarizes the test scenarios used to evaluate the control strategies. The initial values of $CA50$ and $IMEP$ are set at 365.5 CAD and 9.14 bar, respectively, across all scenarios. Tests 0 and 1 correspond to mid-load operating conditions, while the remaining tests cover mid- to high-load conditions. The results of the PI and AMPC strategies are represented in blue and green, respectively, for all test cases except Test 0.

Test 0 is a preliminary validation case, wherein the AMPC controller is assessed using the RTM as the plant. This setup is intended to verify the internal consistency and baseline performance of the control system under idealized conditions, where the prediction model and the plant

Table 2
The Wärtsilä SCRE W31DF engine specifications for the UVATZ model.

Systems	Configuration
Displacement & nominal speed	32.45 l / 720 rpm
Stroke/bore	1.39
Air system	External air compressor with air temperature and pressure control (up to 10 bar)
HRF system	ISO 8217-compliant LFO; common rail 2.0 with twin-needle injector; and multi-injection capability
LRF system	ISO 8217-compliant LNG (MN = 80); low-pressure, multi-point, upstream of the intake valves
Valvetrain	Four valves; variable intake valve closure (VIC)
Control system	Speedgoat rapid control platform

Table 3
Summary of test scenarios and operating conditions.

Load case	Test case with setpoint variation condition	Setpoint changes		Disturbance			
		$CA50$ (CAD)	$IMEP$ (bar)	T_{int} (K)		M_{EGR} (kg)	
				μ	σ	μ	σ
Mid-load (AMPC with RTM as the plant)	Test 0 (Seq. & Sim.)	-1	+1	–	–	–	–
Mid-load	Test 1 (Seq. & Sim.)	-1	+1	–	–	–	–
Mid- to high-load	Test 2 (Seq. & Sim.)	-1	+7	–	–	–	–
Mid- to high-load + disturbance	Test 3 (Seq. & Sim.)	-1	+7	0	1	0	0.0001
Mid- to high-load + strict constraints	Test 4 (Sim.)	-1	+7	–	–	–	–

Legend: Seq.-Sequential, Sim.-Simultaneous

are perfectly matched. In Test 1, step changes in the reference signals are applied, either simultaneously or sequentially, to evaluate the controllers' ability to handle setpoint changes occurring at the same or different times. Test 2 extends this evaluation to higher load conditions, where $IMEP$ is increased by 7 bar using the same ramping strategy as in earlier tests. Test 3 incorporates disturbances in intake temperature (T_{int}) and EGR mass flow (M_{EGR}) to assess the controllers' disturbance rejection capabilities. Finally, Test 4 imposes stricter actuator rate constraints to evaluate the robustness of the controllers under more demanding conditions.

The two scenarios of sequential and simultaneous changes of setpoints were also selected in all tests to evaluate the controllers' ability to manage both isolated and coupled transients, which are representative of real engine operation where load and combustion phasing may change independently or concurrently.

4. Simulation results and comparative analysis

This section presents the validation and performance evaluation of the developed control strategies through MiL simulations. Section 4.1 discusses the tuning of controller parameters to ensure that each controller operates under near-optimal conditions. Section 4.2 presents the results of the AMPC when the RTM is used as the plant model, including its performance under two distinct test conditions: simultaneous changes in setpoints, and independent changes occurring at different times. The subsequent subsections present the results of closed-loop simulations using the UVATZ model as the plant. In each case, the performance of both the PI and AMPC controllers is analyzed and compared.

As will be demonstrated, the AMPC achieves satisfactory performance relative to the model-free PI controllers. The current implementation focuses on a two-input, two-output configuration, but future work will extend the control system to more complex scenarios involving additional actuators and combustion metrics.

Table 4
Tuned parameters for PI controllers.

Controller	P	I	Sampling time [s]
$CA50$ controller	0.005	0.009	1
$IMEP$ controller	500	2000	1

4.1. Controller parameter tuning

The PI controllers are initially tuned under Test 1 conditions and subsequently validated across a range of transient operating scenarios, as summarized in Table 3. Table 4 shows the final tuning parameters for both control loops, with a uniform sampling time of 1 second applied throughout.

The final AMPC tuning parameters are selected to ensure a balance between tracking performance, disturbance rejection, and computational feasibility. Table 5 summarizes these parameters.

4.2. Adaptive model predictive control performance under ideal model conditions

The first validation step evaluates the AMPC in an idealized environment where the RTM acts as the plant. This configuration eliminates model-plant mismatch, enabling an assessment of the controller's intrinsic performance without external uncertainties. Such an analysis is essential to establish a performance baseline before introducing real-world complexities.

Two transient scenarios are considered (Test 0 in Table 3): (i) sequential setpoint changes in $IMEP$ and $CA50$; and (ii) simultaneous setpoint changes in both variables. These scenarios were chosen to reflect representative engine operating conditions, where load ($IMEP$) and combustion phasing ($CA50$) may vary independently or concurrently.

Table 5
Tuned parameters for AMPC controller.

Prediction horizon (N_p) [cycles]	Control horizon (N_c) [cycles]	Q	R	Sampling time [s]
10	3	[160 430]	$[10^{-10}\ \ 1.1\times10^{5}]$	1

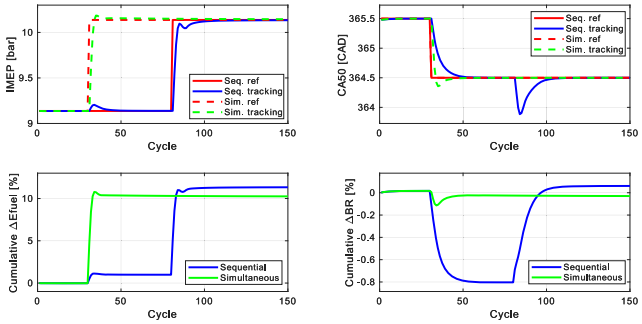

Fig. 5. Test 0-AMPC performance under ideal model conditions.

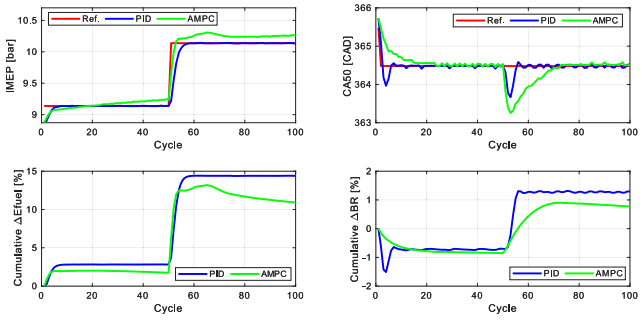

Fig. 6. Test 1-Controller performance under mid-load transients: sequential setpoint changes.

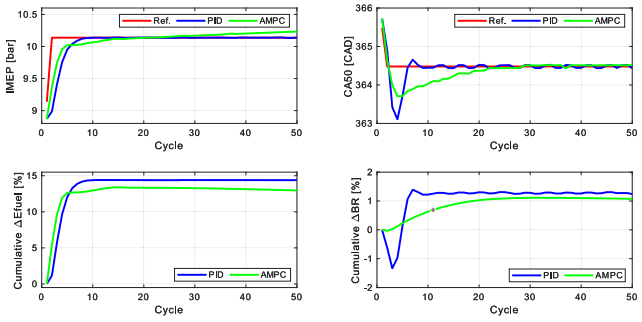

Fig. 7. Test 1-Controller performance under mid-load transients: simultaneous setpoint changes.

Evaluating both isolated and coupled transients provides insight into the controller's ability to manage multivariable interactions effectively.

As shown in Fig. 5, the AMPC achieves zero steady-state error for both $IMEP$ and $CA50$ in all cases, while maintaining desirable transient characteristics. In the sequential setpoint change scenario, a 1 CAD reduction in $CA50$ results in a 0.8% decrease in BR and a 1% increase in ΔE_{fuel}. These adjustments temporarily raise $IMEP$ by 0.1 bar, while $CA50$ converges to its target within approximately 15 engine cycles. Subsequently, at 80 seconds, a 1-bar increase in $IMEP$ reference is achieved through an 11.2% increase in ΔE_{fuel}, which induces a 0.6 CAD undershoot in $CA50$ and an $IMEP$ settling time of about 15 cycles.

In contrast, simultaneous setpoint changes lead to faster convergence: $IMEP$ settles within five cycles and $CA50$ settles within 10 cycles. For instance, when the $IMEP$ reference increases at 30 seconds, the controller responds by increasing fuel energy input while reducing ΔBR. This coordinated adjustment causes a brief $CA50$ deviation before stabilization, highlighting the inherent coupling between control inputs. $IMEP$ consistently converges faster than $CA50$, which can be attributed to the direct proportionality between ΔE_{fuel} and $IMEP$, as well as the higher fidelity of $IMEP$ dynamics in the RTM.

These results confirm that the AMPC can deliver accurate and stable tracking under ideal conditions, validating the internal consistency of the control design. The observed performance - fast $IMEP$ response, acceptable $CA50$ dynamics, and smooth input trajectories - provides a strong baseline before subsequent tests introducing model-plant mismatch and disturbances.

4.3. Controller performance under mid-load transients

This section evaluates the controllers' performance under mid-load conditions, focusing on their ability to manage sequential and simultaneous setpoint changes (Test 1 in Table 3). These scenarios represent realistic engine transients where combustion phasing and load vary either independently or concurrently, providing insight into control robustness under practical operating conditions.

In the first scenario (Fig. 6), the $CA50$ reference is reduced by 1 CAD at 1 second, followed by a 1-bar increase in $IMEP$ reference at 50 seconds. These changes mimic typical engine operations where combustion phasing adjustments precede load variations.

Following the $CA50$ reduction, both controllers respond by increasing ΔE_{fuel} and decreasing ΔBR, which induces a slight $IMEP$ fluctuation due to coupling effects. When the $IMEP$ reference rises, both ΔE_{fuel} and ΔBR increase substantially, causing a temporary $CA50$ drop before stabilization.

Quantitatively, the PI controller achieves an $IMEP$ settling time of six cycles with a mean absolute error (MAE) of 0.0024 bar, while $CA50$ settles in nine cycles with an MAE of 0.025 CAD. The AMPC exhibits a faster $IMEP$ rise time but with a slightly higher MAE of 0.08 bar, reflecting its aggressive ΔE_{fuel} adjustment and modest 1% increase in ΔBR. This behavior underscores the dominant influence of fuel energy on $IMEP$ dynamics. For $CA50$, the AMPC's gradual ΔBR reduction results in slower convergence, though its MAE (0.039 CAD) remains comparable to PI.

The second scenario (Fig. 7) examines simultaneous changes in $IMEP$ and $CA50$ references at 1 second, representing aggressive transients often encountered in real engine operation.

The PI controller achieves settling times of eight cycles for $IMEP$ and nine cycles for $CA50$, with MAEs of 0.0029 bar and 0.038 CAD, respectively. The AMPC exhibits similar qualitative behavior but with slightly longer settling times and higher steady-state errors: 0.0533 bar for $IMEP$ and 0.039 CAD for $CA50$.

Control actions (Fig. 7) reveal that AMPC initially increases ΔE_{fuel} more rapidly, resulting in a total rise of 13.3%, compared to 14.4% for PI–indicating marginally better fuel efficiency. However, AMPC adjusts ΔBR more conservatively, which prolongs $CA50$ convergence. In contrast, PI applies aggressive ΔBR corrections, causing $CA50$ fluctuations and an initial undershoot.

The RTM within the AMPC does not fully capture all UVATZ dynamics, but the controller demonstrates robustness by effectively handling unmodelled dynamics and structural uncertainties. Compared to PI, which achieves slightly faster convergence and marginally better accuracy, AMPC prioritizes fuel efficiency and smoother actuator

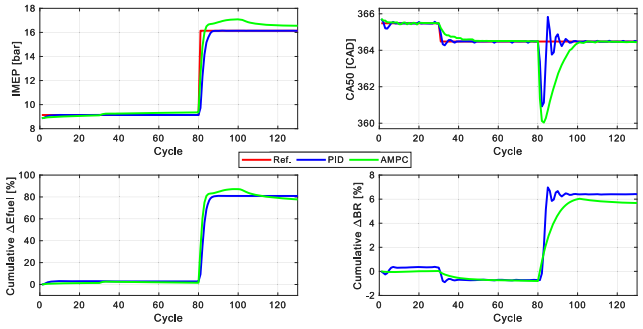

Fig. 8. Test 2-Controller performance under mid- to high-load transients: Sequential setpoint changes.

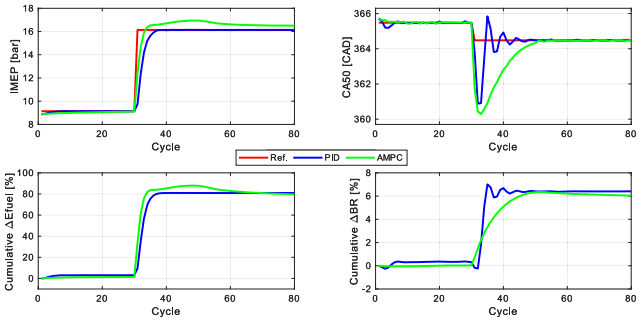

Fig. 9. Test 2-Controller performance under mid- to high-load transients: Simultaneous setpoint changes.

trajectories. PI's performance advantage comes at the cost of significantly higher fuel input and greater $CA50$ variability, whereas AMPC achieves comparable accuracy with lower energy demand. This highlights its suitability for scenarios where efficiency and actuator longevity are critical.

Notably, however, Fig. 7 reveals $IMEP$ divergence in the AMPC case after initial convergence. This is caused by the UVATZ model's sensitivity to small input changes, emphasizing the need for frequent RTM updates to maintain prediction accuracy. Overall, under mid-load conditions, AMPC offers a balanced trade-off between efficiency and control stability, while PI remains preferable when rapid response is the primary objective.

4.4. Controller performance under mid- to high-load transients

Test 2 evaluates controller performance under more demanding conditions involving large $IMEP$ changes. Two scenarios are considered (Test 2 in Table 3): (i) sequential setpoint changes, where $CA50$ is reduced by 1 CAD at 30 seconds followed by a 7-bar $IMEP$ increase at 80 seconds (Fig. 8); and (ii) simultaneous changes, where both references shift at 30 seconds (Fig. 9). These conditions represent aggressive transients typical of high-load engine operation.

In both scenarios, AMPC tracks $IMEP$ setpoints faster than PI, but with a slightly higher steady-state error. For $CA50$, AMPC converges more slowly yet achieves a lower final error than PI. Control input analysis shows that AMPC requires lower final values for both ΔE_{fuel} and ΔBR, reflecting its cost function's emphasis on minimizing actuator effort. PI, in contrast, applies more aggressive corrections, leading to higher fuel input and greater $CA50$ variability.

Under large transients, the trade-off between responsiveness and efficiency becomes more pronounced. PI offers quicker convergence but at the expense of higher fuel demand and less stable combustion phasing. AMPC, while slightly slower in $CA50$ response, delivers smoother control actions and superior energy efficiency. These are critical advantages under high-load conditions where actuator stress and fuel economy are major concerns. These results confirm that AMPC can maintain stable and efficient control during aggressive load changes, provided that its slower $CA50$ dynamics are acceptable for the application.

4.5. Robustness to disturbances under mid- to high-load conditions

Test 3 evaluates controller performance under mid- to high-load conditions with random disturbances in intake temperature (T_{int}) and EGR mass flow (M_{EGR}). Two scenarios are considered (Test 3 in Table 3): (i) sequential setpoint changes, where $CA50$ is reduced by 1 CAD at 1 second followed by a 7-bar $IMEP$ increase at 50 seconds (Fig. 10); and (ii) simultaneous changes, where both references shift at 1 second (Fig. 11).

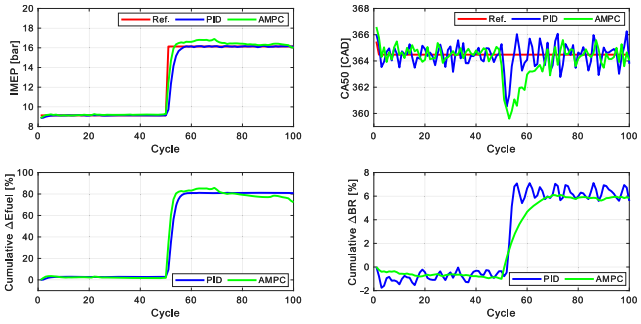

Fig. 10. Test 3-Disturbance scenario: Sequential setpoint changes.

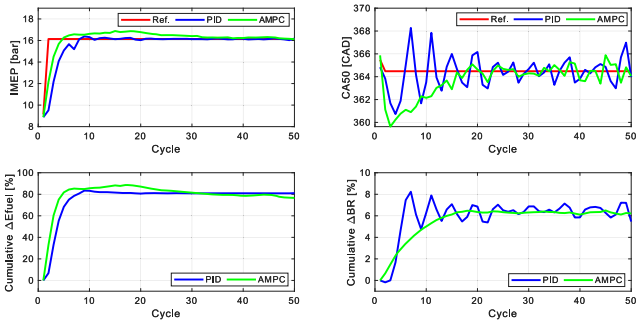

Fig. 11. Test 3-Disturbance scenario: Simultaneous setpoint changes.

These conditions represent some of the most challenging operating environments for RCCI control.

In the sequential case (Fig. 10), disturbances cause noticeable $CA50$ fluctuations, particularly for PI, reflecting its limited high-frequency disturbance rejection and high-pass response characteristics. AMPC maintains better $CA50$ stability, with a steady-state MAE of 0.38 CAD versus 0.58 CAD for PI, while $IMEP$ remains relatively smooth for both controllers, with MAEs of 0.02 bar for PI and 0.2 bar for AMPC. AMPC responds to $IMEP$ increases with significant ΔE_{fuel} adjustments and modest ΔBR changes, resulting in temporary $CA50$ advancement and slight $IMEP$ overshoot.

When both setpoints change simultaneously (Fig. 11), AMPC achieves faster $IMEP$ response and lower $CA50$ variability than PI, but PI maintains slightly better $IMEP$ accuracy. Control actions reveal that AMPC applies smoother and more efficient adjustments, whereas PI relies on abrupt corrections, increasing actuator stress and fuel demand.

Table 6 confirms these trends. AMPC settles $IMEP$ in six cycles versus 11 for PI, while both require 20 cycles for $CA50$. AMPC also uses less fuel energy (77.8% vs. 80.9%), reinforcing its efficiency advantage despite a slightly higher $IMEP$ steady-state error (0.32 bar vs. 0.04 bar).

Table 6
Performance metrics under disturbance conditions.

Controller	$IMEP$ settling time (cycles)	$CA50$ settling time (cycles)	$IMEP$ steady-state error (bar)	$CA50$ steady-state error (CAD)	Final $\mathbf{\Delta E_{fuel}}(\%)$
PI	11	20	0.04	0.74	80.9%
AMPC	6	20	0.32	0.45	77.8%

Table 7
Summary of tracking accuracy and fuel efficiency across all tests.

Test	Controller	$IMEP$ settling time (cycles)	$CA50$ settling time (cycles)	Final $\mathbf{\Delta E_{fuel}}(\%)$
Test 1 (Seq.)	PI	6	9	14.5
	AMPC	2	23	11
Test 1 (Sim.)	PI	8	9	14.4
	AMPC	13	22	13.3
Test 2 (Seq.)	PI	6	9	80
	AMPC	2	22	77
Test 2 (Sim.)	PI	6	18	80
	AMPC	2	21	79
Test 3 (Seq.)	PI	6	6	80
	AMPC	2	3	75
Test 3 (Sim.)	PI	11	20	80.9
	AMPC	6	20	77.8
Test 4 (Sim.)	PI	20	25	80
	AMPC	30	25	78
Average	PI	**9**	**14**	**61.4**
	AMPC	**8**	**19**	**58.7**

Overall, these results show that under disturbance-rich conditions, AMPC provides superior $CA50$ stability and energy efficiency. PI offers marginally better $IMEP$ accuracy, but at the cost of higher fuel consumption and aggressive actuator usage. AMPC's optimization-based strategy delivers smoother control actions and reduces actuator stress, making it more suitable for scenarios prioritizing robustness and efficiency over minimal $IMEP$ error.

4.6. Controller performance under actuator rate constraints

One of AMPC's key advantages is its ability to explicitly handle constraints on both control inputs and system states - something inherently challenging for PI controllers. Test 4 demonstrates this capability by introducing strict limits on the rate of change for control inputs within the AMPC framework. These constraints are critical for real-world engine operation, where actuator limitations and combustion safety must be respected.

Fig. 12 shows the results of Test4ıs stricter constraints. As expected, the constrained AMPC (AMPC-Constrained) exhibits slower responses in both ΔE_{fuel} and ΔBR, leading to delayed convergence of $IMEP$ and $CA50$ compared to the unconstrained case. This delay, however, illustrates a valuable capability: the ability to shape combustion dynamics conservatively, for example, by limiting heat release rate and peak pressure rise rate. Both are key factors for achieving efficient and low-emission RCCI combustion.

The imposed limits result in an initial $IMEP$ overshoot of about 0.25 bar and a $CA50$ undershoot of roughly 2 CAD before stabilization. The overall settling time extends to around 30 seconds, primarily governed by the input rate constraints. Relaxing these limits would reduce the delay but at the expense of more aggressive combustion dynamics. Although the current two-degree-of-freedom (2-DoF) control structure does not fully showcase AMPC's potential, these results highlight its flexibility in managing constraints–a capability that PI lacks. Furthermore, the strong correlation between $IMEP$ and ΔE_{fuel} tends to dominate system dynamics, reducing the influence of BR during load transients. Enhancing the RTM's sensitivity to BR and integrating a data-driven $CA50$ model could further enhance prediction accuracy and control performance.

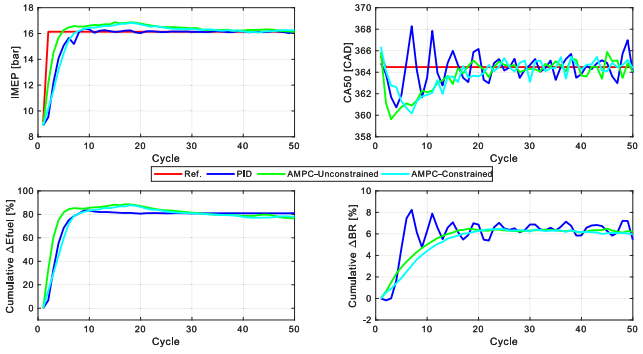

Fig. 12. Test 4-Impact of actuator rate constraints on AMPC performance.

Overall, AMPC's ability to enforce input rate constraints enables safer and more controlled combustion shaping, which is essential for practical engine applications. This comes at the expense of slower response, but provides a critical advantage over PI in terms of operational safety and adaptability.

4.7. Summary of tracking accuracy and energy efficiency

The performance of both controllers was evaluated in a range of MiL test cases covering mid-load and mid-to-high-load operating points, including scenarios with disturbances and actuator constraints. Table 7 summarizes the results. $IMEP$ tracking was generally accurate for both approaches, with steady-state errors well below 0.4 bar, and $CA50$ errors staying under 0.8 CAD in all cases.

On average, PI achieved slightly faster $CA50$ settling (14 cycles vs. 19 cycles for AMPC) but slightly slower $IMEP$ settling (nine cycles vs. eight cycles for AMPC). In contrast, AMPC delivered lower final fuel input (58.7% vs. 61.4%) and maintained smoother actuator trajectories. These results reflect the inherent design priorities of each controller: PI favors responsiveness, while AMPC prioritizes efficiency and constraint handling.

In test cases 1–4, slight overshoot by the AMPC can be observed during setpoint changes. The overshoot of $IMEP$ remains below 1 bar

in all cases. The overshoot of $CA50$ remains below 2 CAD when a set-point change is not applied to $IMEP$. The highest overshoots of $CA50$, which are caused by the strong coupling effect of ΔE_{fuel}, remain below 5 CAD. To the authors' knowledge, no numerical overshoot limits for $IMEP$ and $CA50$ have been clearly reported in marine engines (e.g. International Maritime Organization (IMO) & U. S. EPA, 2022). The overshoot of the aforementioned variables in RCCI automotive engines has been reported to be near zero (Amini et al., 2018; Raut et al., 2018). Considering the real marine engine combustion, where process disturbances and system constraints are present (test cases 3 and 4), the obtained values, excluding the coupling effects, are well in line with the safety standards of current marine engines.

Scenario-specific results confirm these patterns. PI performed well in moderate transients but consumed more fuel and exhibited greater variability under disturbances. AMPC demonstrated robustness, smoother actuator trajectories, and the ability to enforce input rate limits. These capabilities are essential for practical RCCI control where stability and fuel economy are critical. PI was more responsive in low-to-moderate transients but exhibited greater variability and higher fuel use under disturbances.

5. Conclusions and outlook

The key outcomes of this study can be summarized according to the relevant characteristics of the developed Adaptive Model Predictive Control (AMPC) framework. These findings highlight the contribution to contemporary control theory and its practical significance for reactivity-controlled compression ignition (RCCI) engine control.

- **Validity of the observer:** The real-time model (RTM) reliably replicated combustion indicators from the detailed UVATZ (University of Vaasa Advanced Thermo-Kinetic Multi-zone) model while offering a two-order-of-magnitude reduction in computational cost. Its suitability for control design was validated in all model-in-the-loop (MiL) simulations, but improving the prediction accuracy of the crank angle at 50% mass fraction burned ($CA50$) remains a priority for future work.
- **Linearity and adaptiveness:** The RTM's linear structure enabled the formulation of a linear AMPC, while its parameter-varying capability supported adaptive control across multiple operating points without compromising real-time performance.
- **Toolchain implementation:** The complete model-based RCCI control toolchain was successfully implemented and validated through MiL simulations targeting marine engine applications. Despite its model-based nature, the AMPC demonstrated strong robustness against unstructured uncertainties.
- **Controller comparison:** Both proportional-integral (PI) and AMPC controllers achieved comparable tracking accuracy across all test cases. However, the AMPC showed faster indicated mean effective pressure ($IMEP$) response, lower $CA50$ steady-state error, and improved fuel efficiency, achieving lower final fuel input in all scenarios. It also handled white-noise disturbances from a 10% change in intake temperature and internal exhaust gas recirculation (EGR) variations more effectively than PI.
- **Tuning effort:** The PI controller required extensive manual tuning, whereas the AMPC delivered strong performance with minimal tuning effort.
- **Scalability:** While the AMPC's advantages were moderate in the current two-degree-of-freedom (2-DoF) configuration, they are expected to become more pronounced in higher-DoF systems. Future extensions should consider additional objectives such as emissions control and fuel efficiency.
- $CA50$ **model fidelity:** The current $CA50$ model offers a simplified representation of mid- and mid- to high-load combustion behavior. Incorporating a more accurate, potentially data-driven $CA50$ model could enhance AMPC tracking performance.
- **Future implementation:** The proposed control strategies will be experimentally validated on a real-world test bench at the University of Vaasa (UVA) Energylab using a Wärtsilä 4L20 engine, where one cylinder is retrofitted for RCCI operation. The AMPC framework has already been implemented on a rapid control prototyping (RCP) platform, enabling its deployment on this setup and facilitating future engine-in-the-loop (EiL) testing and validation.

In summary, the proposed AMPC successfully achieved the dual control objectives of $IMEP$ and $CA50$ tracking by optimally managing the energy split between diesel and gas fuels. While both controllers performed well in MiL simulations, the AMPC demonstrated better responsiveness, robustness, and fuel efficiency. Its adaptability and reduced tuning requirements make it a promising candidate for real-time engine control, particularly in high-DoF systems where emissions and energy efficiency are critical.

CRediT authorship contribution statement

Xiaoguo Storm: Writing – original draft, Validation, Software, Methodology, Formal analysis, Data curation; **Amir-Mohammad Shamekhi:** Writing – review & editing, Writing – original draft, Validation, Supervision, Methodology, Formal analysis, Conceptualization; **Mohammad Raisi Esfarjani:** Writing – review & editing, Visualization, Validation, Software; **Amin Modabberian:** Writing – review & editing, Software, Resources; **Aneesh Vasudev:** Software, Resources, Investigation, Data curation; **Kai Zenger:** Supervision, Project administration, Funding acquisition; **Jari Hyvönen:** Resources, Project administration, Funding acquisition; **Maciej Mikulski:** Writing – review & editing, Supervision, Resources, Project administration, Methodology, Funding acquisition, Formal analysis.

Declaration of competing interest

The authors declare that they have no known competing financial interests or personal relationships that could have appeared to influence the work reported in this paper.

Acknowledgement

The work was conducted within the framework of the Clean Propulsion Technologies project, with financial support from Business Finland (ref. 38485/31/2020).

Appendix A. Comparison of MPC, PI, and Alternative Control Strategies

In industrial practice, PI/PID and Model Predictive Control (MPC) represent two dominant but complementary paradigms. PI/PID remains the backbone of regulatory control due to simplicity, low commissioning cost, transparency, and universal availability in industrial platforms (Åström & Hägglund, 2001; Skogestad, 2003). MPC, in contrast, has become the preferred solution for constrained multivariable systems where interaction management and operation near physical limits are central concerns (Mayne et al., 2000; Qin & Badgwell, 2003; Rawlings et al., 2017).

PI control requires limited plant knowledge and can achieve satisfactory robustness within moderate uncertainty ranges when properly tuned (Åström & Hägglund, 2001; Skogestad, 2003). Its strengths include ease of maintenance, intuitive parameterization, and proven lifecycle reliability. However, it lacks native constraint handling and is less effective for strongly coupled MIMO systems or when operation near hard limits is critical. Anti-windup schemes mitigate saturation effects but do not provide predictive constraint management.

MPC integrates prediction, multivariable coordination, and explicit constraint handling into a single optimization framework (Mayne et al., 2000; Rawlings et al., 2017). Industrial surveys confirm its widespread deployment, particularly in large-scale process industries (Qin & Badgwell, 2003). Linear MPC is often preferred due to convex optimization structure and reliable real-time implementation, while nonlinear MPC is used where strong nonlinearities significantly influence performance (Rawlings et al., 2017). Robustness in MPC depends on modeling quality and design choices (e.g., disturbance modeling, terminal ingredients, or robust formulations) rather than receding-horizon operation alone (Mayne et al., 2000; Rawlings et al., 2017). Adaptive MPC extends applicability to slowly varying plants but increases identification and validation complexity.

Beyond PI and MPC, several controller families are widely used in specific industrial domains.

Robust linear control (H∞, μ-synthesis) provides systematic treatment of model uncertainty and disturbance attenuation through worst-case formulations (Doyle et al., 1988; Zhou et al., 1996). These methods are prevalent in aerospace and precision motion systems, where formal robustness guarantees are required. However, controller order may be high, uncertainty modeling demands care, and constraint handling is typically external to the design.

LQR/LQG offers computational simplicity and effective nominal multivariable control when reliable state-space models are available (Anderson & Moore, 2007). Nevertheless, these methods do not inherently address constraints and may be sensitive to plant uncertainty and saturation. Doyle's well-known result demonstrates that LQG does not guarantee universal robustness margins (Doyle, 1978), motivating the use of robust control methods for uncertain plants. In practice, LQR/LQG is often used as an inner-loop stabilizing element rather than a supervisory controller.

Gain scheduling is widely adopted for systems operating across broad envelopes (e.g., aircraft, gas turbines, engines) because it preserves a low computational burden and engineering transparency (Leith & Leithead, 2000; Rugh & Shamma, 2000). However, global stability and robustness are not automatically guaranteed, particularly in ad hoc implementations. LPV synthesis methods provide formal guarantees within structured parameter-dependent models (Apkarian et al., 1995), albeit at increased modeling and synthesis effort. In both cases, constraint handling typically requires additional mechanisms.

Nonlinear Lyapunov-based methods (e.g., backstepping, feedback linearization) provide constructive stability guarantees under structural assumptions (Khalil, 2002; Krstic et al., 1995). These approaches are powerful when accurate nonlinear models and full state information are available. However, implementation complexity and sensitivity to modeling errors limit widespread industrial use. Constraints and actuator limits must generally be handled separately.

Sliding Mode Control (SMC) offers strong robustness to matched uncertainties and disturbances (Utkin, 2013). Higher-order formulations reduce chattering (Levant, 2005), yet noise sensitivity, actuator wear, and implementation challenges under sampling and delay remain practical concerns (Richard et al., 2001). Consequently, SMC is common in power electronics and motion control but less prevalent in process industries.

Two practical augmentation strategies are worth highlighting. Reference governors enforce constraints by modifying reference trajectories for a pre-stabilized controller, offering a retrofit solution when full MPC redesign is impractical (Bemporad, 1998; Garone et al., 2017). However, achievable performance is typically inferior to integrated constrained optimization. Disturbance observer-based control (DOBC) and active disturbance rejection control (ADRC) improve robustness by estimating and compensating aggregate disturbances (Chen et al., 2016; Gao, 2015; Han, 2009). These approaches are widely used in motion systems but require careful bandwidth tuning and do not intrinsically handle hard constraints.

Finally, data-driven methods (fuzzy control, neural networks, reinforcement learning) are increasingly explored when first-principles modeling is difficult (MAMDANI, 1974; Narendra, 1989). While such methods can approximate complex nonlinear behaviors, stability guarantees, safety certification, and constraint enforcement remain active research challenges, particularly for reinforcement learning (Garcıa & Fernández, 2015). Industrial deployment typically favors hybrid architectures in which learning augments rather than replaces conventional feedback control.

Overall, PI/PID dominates simple regulatory loops due to unmatched simplicity and maintainability, whereas MPC dominates constrained multivariable applications requiring systematic coordination. Robust, nonlinear, and adaptive approaches are highly valuable in specialized domains but often involve greater modeling effort, validation complexity, or implementation burden. In practice, hybrid architectures combining robust estimation, constraint management, and conventional feedback are increasingly common in modern industrial systems.

Now, the selection of Adaptive MPC for one engine-control structure and PI control for the alternative structure is directly supported by the comparative analysis summarized in Table A.8.

Engine combustion control (e.g., $CA50$, $IMEP$, emissions-efficiency trade-offs) is inherently multivariable, constraint-driven, and operating-point dependent. As highlighted in Table A.8, MPC is one of the few strategies that provides native constraint handling, systematic multivariable coordination, and structured treatment of model uncertainty through robust or adaptive extensions (Mayne et al., 2000; Qin & Badgwell, 2003; Rawlings et al., 2017). In engine applications, actuator limits, rate constraints, and combustion stability boundaries are critical; therefore, predictive constraint management is essential rather than optional. The adaptive extension further improves performance under varying operating conditions (speed/load transients, fuel variations), addressing the moderate-to-high model uncertainty typical of combustion systems (Ioannou & Sun, 1996), while maintaining the constraint-handling capability unique to MPC. According to Table A.8, this combination (Adaptive MPC) scores high in constraint capability and uncertainty accommodation, justifying its use for the more demanding control structure.

In contrast, the alternative structure targets a control objective that is less constraint-intensive and more localized. As summarized in Table A.8, PI control offers very high industrial maturity, minimal implementation burden, and sufficient robustness under moderate uncertainty when properly tuned (Åström & Hägglund, 2001; Skogestad, 2003). For single-loop or weakly coupled dynamics where predictive coordination is not critical, PI remains the most cost-effective and maintainable solution. Its extremely low computational and commissioning complexity makes it appropriate when full predictive optimization is not justified by performance gains.

Therefore, the selection reflects a complexity-capability trade-off consistent with the comparative assessment.

- When multivariable interaction, hard constraints, and operating-point variability dominate, Adaptive MPC is justified.
- When the control task is structurally simpler and robustness margins are sufficient, PI control is the pragmatic and industrially aligned choice.

This dual-structure approach aligns with established industrial practice, where advanced predictive control is deployed selectively for

Table A.8
Performance and implementation comparison of PI, MPC, and alternative control strategies.

Strategy	Robustness to Model Error	Native Constraint Handling	Uncertainty Treatment	Industrial Maturity	Implementation Effort	References
PI/PID	Moderate (tuning-based)	No (anti-windup only)	Implicit margins	Very High	Very Low	(Åström & Hägglund, 2001; Skogestad, 2003)
Linear MPC	Moderate-High (design-dependent)	Yes	Model-based; robust/adaptive variants	High (process industries)	Medium	(Ioannou & Sun, 1996; Mayne et al., 2000; Rawlings et al., 2017)
Nonlinear MPC	Moderate-High	Yes	Nonlinear prediction; robust extensions	Moderate	High	(Rawlings et al., 2017)
Robust H∞ / μ	High (worst-case design)	No (external supervision)	Explicit uncertainty modeling	Moderate-High (aerospace / precision)	High	(Doyle et al., 1988; Zhou et al., 1996)
LQR	Moderate (nominal optimal)	No	Model-based optimal control	Moderate	Low-Medium	(Anderson & Moore, 2007)
LQG	Moderate-Low (uncertainty-sensitive)	No	Estimator-based optimal control	Moderate	Medium	(Doyle, 1978)
Gain Scheduling	Moderate (validation-driven)	No	Local linear robustness	High (aerospace / engines)	Medium	(Leith & Leithead, 2000; Rugh & Shamma, 2000)
LPV (guaranteed)	Moderate-High (within LPV set)	No	Structured parametric uncertainty	Moderate	High	(Apkarian et al., 1995)
Nonlinear Lyapunov (Backstepping/FL)	Moderate (model-dependent)	No	Structural nonlinear design	Selective	High	(Khalil, 2002; Krstic et al., 1995)
Passivity-Based Control	Moderate-High (energy-based robustness)	No	Physical structure exploitation	Selective	Medium-High	(Ortega et al., 2002)
Sliding Mode	High (matched uncertainty)	Limited (via saturation)	Switching robustness	Selective (power/motion)	Medium-High	(Levant, 2005; Utkin, 2013)
Reference Governor	Moderate (baseline dependent)	Yes (explicit constraint enforcement)	Constraint supervision layer	Moderate	Medium	(Bemporad, 1998; Garone et al., 2017)
DOBC/ADRC	Moderate-High (disturbance rejection)	No	Disturbance estimation & compensation	Moderate-High (motion systems)	Medium	(Chen et al., 2016; Gao, 2015; Han, 2009)
Fuzzy Control	Variable (rule-based)	Limited	Heuristic / knowledge-based	Selective	Medium	(MAMDANI, 1974)
Neural Control	Variable (data-dependent)	Limited	Learned nonlinear mapping	Selective	Medium-High	(Narendra, 1989)
Reinforcement Learning	Variable (safety-dependent)	Emerging (safe RL research)	Policy learning under uncertainty	Emerging	High	(Garcıa & Fernández, 2015)

performance-critical subsystems, while classical PI remains the backbone of simpler regulatory loops.

References

Amini, M. R., Shahbakhti, M., & Sun, J. (2018). Predictive second order sliding control of constrained linear systems with application to automotive control systems. In *2018 Annual american control conference (ACC)* (pp. 1629–1634). https://doi.org/10.23919/ACC.2018.8431559

Anderson, B. D. O., & Moore, J. B. (2007). Optimal control: linear quadratic methods. Courier Corporation.

Apkarian, P., Gahinet, P., & Becker, G. (1995). Self-scheduled h∞ control of linear parameter-varying systems: A design example. *Automatica*, *31*(9), 1251–1261. https://doi.org/10.1016/0005-1098(95)00038-X

Arora, J. K., & Shahbakhti, M. (2017). Real-time closed-loop control of a light-duty RCCI engine during transient operations. Technical Report SAE Technical Paper.

Åström, K. J., & Hägglund, T. (2001). The future of PID control. *Control Engineering Practice*, *9*(11), 1163–1175. PID Control. https://doi.org/10.1016/S0967-0661(01)00062-4

Basina, L. N. A. (2019). Modeling and control of maximum pressure rise rate in RCCI engines. Master's thesis. Michigan Technological University.

Basina, L. N. A., Irdmousa, B. K., Velni, J. M., Borhan, H., Naber, J. D., & Shahbakhti, M. (2020). Data-driven modeling and predictive control of maximum pressure rise rate in RCCI engines. In *2020 IEEE Conference on control technology and applications (CCTA)* (pp. 94–99). IEEE.

Batool, S., Naber, J., & Shahbakhti, M. (2023). Closed-loop predictive control of a multi-mode engine including homogeneous charge compression ignition, partially premixed charge compression ignition, and reactivity controlled compression ignition modes. *SAE International Journal of Fuels and Lubricants*, *16*(1), 15–36.

Batool, S., Naber, J. D., & Shahbakhti, M. (2021). Data-driven modeling and control of cyclic variability of an engine operating in low temperature combustion modes. *IFAC-PapersOnLine*, *54*(20), 834–839.

Bemporad, A. (1998). Reference governor for constrained nonlinear systems. *IEEE Transactions on Automatic Control*, *43*(3), 415–419. https://doi.org/10.1109/9.661611

Bozza, F., Teodosio , L., V.D. , Bellis, S. , Fontanesi, A. , Iorio, A refined od turbulence model to predict tumble and turbulence in si engines, *SAE International Journal of Engines*, *12*(1), (2019), 15–30. https://www.jstor.org/stable/26745561

Chang, J., Güralp, O., Filipi, Z., Assanis, D. N., Kuo, T.-W., Najt, P., & Rask, R. (2004). New heat transfer correlation for an HCCI engine derived from measurements of instantaneous surface heat flux. In *2004 Powertrain & fluid systems conference & exhibition*. SAE International. https://doi.org/10.4271/2004-01-2996

Chen, W.-H., Yang, J., Guo, L., & Li, S. (2016). Disturbance-observer-based control and related methods–an overview. *IEEE Transactions on Industrial Electronics*, *63*(2), 1083–1095. https://doi.org/10.1109/TIE.2015.2478397

Cohen, S. D., Hindmarsh, A. C., and Dubois, P. F., Cvode, a stiff/nonstiff ode solver in c, *Computer in Physics*, *10* (2), (1996), 138–143. https://doi.org/10.1063/1.4822377

Doyle, J. (1978). Guaranteed margins for LQG regulators. *IEEE Transactions on Automatic Control*, *23*(4), 756–757.

Doyle, J., Glover, K., Khargonekar, P., & Francis, B. (1988). State-space solutions to standard h2 and h∞ control problems. In *1988 American control conference* (pp. 1691–1696). https://doi.org/10.23919/ACC.1988.4789992

Duraisamy, G., Rangasamy, M., & Nagarajan, G. (2019). Effect of EGR and premixed mass percentage on cycle to cycle variation of methanol/diesel dual fuel RCCI combustion. Technical Report SAE Technical Paper.

Fakhari, A. H., Gharehghani, A., Salahi, M. M., & Andwari, A. M. (2024). Numerical investigation of the hydrogen-enriched ammonia-diesel RCCI combustion engine. *Fuel*, *375*, 132579.

Fakhari, A. H., Gharehghani, A., Salahi, M. M., Mahmoudzadeh Andwari, A. Mikulski, M. Hunicz, J. Könnö, J. (2023). Numerical investigation of ammonia-diesel fuelled engine operated in RCCI mode In *16th International Conference on Engines & Vehicles* SAE International (pp. 24–0057). https://doi.org/10.4271/2023-24-0057

Gao, Z. (2015). Active disturbance rejection control: From an enduring idea to an emerging technology. In *2015 10th international workshop on robot motion and control (romoco)* (pp. 269–282). https://doi.org/10.1109/RoMoCo.2015.7219747

Garcıa, J., & Fernández, F. (2015). A comprehensive survey on safe reinforcement learning. *Journal of Machine Learning Research*, *16*(1), 1437–1480.

Garone, E., Di Cairano, S., & Kolmanovsky, I. (2017). Reference and command governors for systems with constraints: A survey on theory and applications. *Automatica*, *75*, 306–328. https://doi.org/10.1016/j.automatica.2016.08.013

GhafGhanbari, P., Bao, Y., & Velni, J. M. (2024). Uncertainty-aware output feedback model predictive combustion control of RCCI engines. *Control Engineering Practice*, *150*, 106005.

Goodwin, D. G., Moffat, H. K., Schoegl, I., Speth, R. L., & Weber, B. W. (2025). Cantera: An object-oriented software toolkit for chemical kinetics, thermodynamics, and transport processes. https://www.cantera.org. Version 3.2.0. https://doi.org/10.5281/zenodo.17620923

Han, J. (2009). From PID to active disturbance rejection control. *IEEE Transactions on Industrial Electronics*, *56*(3), 900–906. https://doi.org/10.1109/TIE.2008.2011621

International Maritime Organization (IMO) & U. S. EPA (2022). Marpol annex vi - memorandum of understanding (mou). Available online at U.S. EPA website. Accessed: 2026-02-22.

Ioannou, P. A., & Sun, J. (1996). Robust Adaptive Control. Number v. 1 in Robust Adaptive Control. PTR Prentice-Hall. https://books.google.fi/books?id=TIYqAQAAMAAJ.

Irdmousa, B. K., Naber, J. D., & Shahbakhti, M. (2023). Cfd-based data-driven modeling of reactivity and stratification dynamics for rcci engine control. *IFAC-PapersOnLine*, *56*(2), 8272–8277.

Irdmousa, B. K., Naber, J. D., Velni, J. M., Borhan, H., & Shahbakhti, M. (2021). Input-output data-driven modeling and mimo predictive control of an rcci engine combustion. *IFAC-PapersOnLine*, *54*(20), 406–411.

Irdmousa, B. K., Rizvi, S. Z., Veini, J. M., Nabert, J. D., & Shahbakhti, M. (2019). Data-driven modeling and predictive control of combustion phasing for RCCI engines. In *2019 American control conference (ACC)* (pp. 1617–1622). IEEE.

Kakoee, A., Vasudev, A., Smulter, B., Hyvonen, J., & Mikulski, M. (2023). A predictive 1d modeling framework for reactivity-controlled compression ignition engines, via a chemistry-based, multizone combustion object. In *16th international conference on engines & vehicles*. SAE International. https://doi.org/10.4271/2023-24-0001

Khalil, H. K. (2002). Nonlinear systems. Prentice Hall.

Khodadadi Sadabadi, K., Shahbakhti, M., Bharath, A. N., & Reitz, R. D. (2016). Modeling of combustion phasing of a reactivity-controlled compression ignition engine for control applications. *International Journal of Engine Research*, *17*(4), 421–435.

Kondipati, N. N. T., Arora, J. K., Bidarvatan, M., & Shahbakhti, M. (2017). Modeling, design and implementation of a closed-loop combustion controller for an RCCI engine. In *2017 American control conference (ACC)* (pp. 4747–4752). IEEE.

Krstic, M., Kokotovic, P. V., & Kanellakopoulos, I. (1995). Nonlinear and adaptive control design. John Wiley & Sons, Inc.

Lehtoranta, K., Kuittinen, N., Vesala, H., & Koponen, P. (2023). Methane emissions from a state-of-the-art LNG-powered vessel. *Atmosphere*, *14*(5), 825.

Leith, D. J., & Leithead, W. E. (2000). Survey of gain-scheduling analysis and design. *International Journal of Control*, *73*(11), 1001–1025. https://doi.org/10.1080/002071700411304

Levant, A. (2005). Quasi-continuous high-order sliding-mode controllers. *IEEE Transactions on Automatic Control*, *50*(11), 1812–1816. https://doi.org/10.1109/TAC.2005.858646

Li, Y., Jia, M., Liu, Y., & Xie, M. (2013). Numerical study on the combustion and emission characteristics of a methanol/diesel reactivity controlled compression ignition (RCCI) engine. *Applied energy*, *106*, 184–197.

MAMDANI, E. H. (1974). Application of fuzzy algorithms for control of simple dynamic plant. In *Proceedings of the institution of electrical engineers* (pp. 1585–1588). IET (*vol. 121*).

MathWorks (2023). Adaptive MPC. https://se.mathworks.com/help/mpc/ug/\protect\penalty\z@adaptive-mpc.html. Accessed: Nov. 07, 2023.

Mayne, D. Q., Rawlings, J. B., Rao, C. V., & Scokaert, P. O. M. (2000). Constrained model predictive control: Stability and optimality. *Automatica*, *36*(6), 789–814. https://doi.org/10.1016/S0005-1098(99)00214-9

Mikulski, M., Balakrishnan, P. R., Doosje, E., & Bekdemir, C. (2018). Variable valve actuation strategies for better efficiency load range and thermal management in an RCCI engine. Technical Report SAE Technical Paper.

Mikulski, M., & Bekdemir, C. (2017). Understanding the role of low reactivity fuel stratification in a dual fuel RCCI engine–a simulation study. *Applied energy*, *191*, 689–708.

Mikulski, M., Ramesh, S., & Bekdemir, C. (2019). Reactivity controlled compression ignition for clean and efficient ship propulsion. *Energy*, *182*, 1173–1192.

Modabberian, A., Storm, X., Shamekhi, A.-M., Vasudev, A., Zenger, K., Hyvönen, J., & Mikulski, M. (2024). Low temperature combustion modeling and predictive control of marine engines. *Applied Sciences*, *14*(5), 2033.

Narendra, K. S. (1989). Identification and control of dynamical systems using neural networks. *IEEE Transactions on Neural Networks*, *1*(1), 183–192.

Ortega, R., van der Schaft , A., Maschke, B., Escobar, G., Interconnection and damping assignment passivity-based control of port-controlled Hamiltonian systems, *Automatica*, *38* (4), (2002), 585–596. https://doi.org/10.1016/S0005-1098(01)00278-3

Paykani, A., Garcia, A., Shahbakhti, M., Rahnama, P., & Reitz, R. D. (2021). Reactivity controlled compression ignition engine: pathways towards commercial viability. *Applied Energy*, *282*, 116174.

Punasiya, M., & Sarangi, A. K. (2024). Machine learning-based modeling and predictive control of combustion phasing and load in a dual-fuel low-temperature combustion engine. *SAE International Journal of Engines*, *17*(03-17-04-0030), 529–549.

Qin, S. J., & Badgwell, T. A. (2003). A survey of industrial model predictive control technology. *Control Engineering Practice*, *11*(7), 733–764. https://doi.org/10.1016/S0967-0661(02)00186-7

Raut, A., Irdmousa, B. K., & Shahbakhti, M. (2018). Dynamic modeling and model predictive control of an RCCI engine. *Control Engineering Practice*, *81*, 129–144.

Rawlings, J. B., Mayne, D. Q., & Diehl, M. (2017). Model Predictive Control: Theory, Computation, and Design. Nob Hill Publishing. https://books.google.fi/books?id=MrJctAEACAAJ.

Richard, J.-P., Gouaisbaut, F., & Perruquetti, W. (2001). Sliding mode control in the presence of delay. *Kybernetika*, *37*(3), [277]–294. http://eudml.org/doc/33535.

Rugh, W. J., & Shamma, J. S. (2000). Research on gain scheduling. *Automatica*, *36*(10), 1401–1425. https://doi.org/10.1016/S0005-1098(00)00058-3

Sadabadi, K. K. (2015). Modelling and control of combustion phasing of an RCCI engine. *Master of science in mechanical engineering* Houghton, Michigan, USA Michigan Technological University. https://doi.org/10.37099/mtu.dc.etds/966

Sadabadi, K. K., & Shahbakhti, M. (2016). Dynamic modelling and controller design of combustion phasing for an RCCI engine. In *Asme 2016 dynamic systems and control conference: American society of mechanical engineers*.

Saxena, M. R., Suman, S., & Maurya, R. K. (2022). An Assessment of Cyclic Variations in the Air-Fuel Ratio for RCCI Engine. Technical Report SAE Technical Paper.

Skogestad, S. (2003). Simple analytic rules for model reduction and PID controller tuning. *Journal of Process Control*, *13*(4), 291–309. https://doi.org/10.1016/S0959-1524(02)00062-8

Storm, X., Vasudev, A., Shamekhi, A.-M., Modabberian, A., Zenger, K., Hyvönen, J., & Mikulski, M. (2023). Real-time predictive model for reactivity controlled compression ignition marine engines. *Control Engineering Practice*, *141*, 105724.

Y. , Sun, R.D. , Reitz, Modeling diesel engine nox and soot reduction with optimized two-stage combustion. In SAE 2006 world congress & exhibition, *SAE International*, (2006). https://doi.org/10.4271/2006-01-0027

Utkin, V. I. (2013). Sliding modes in control and optimization. Springer Science & Business Media.

Vasudev, A., Cafari, A., Axelsson, M., Mikulski, M., & Hyvonen, J. (2022a). Towards next generation control-oriented thermo-kinetic model for reactivity controlled compression ignition marine engines. Technical Report SAE Technical Paper.

Vasudev, A., Kakoee, A., Axelsson, M., Almani, H. M., Hyvönen, J., & Mikulski, M. (2024). Advancing autonomy of chemical kinetics based multizone models for reactivity controlled compression ignition engines. *Energy Conversion and Management*, *312*, 118562.

Vasudev, A., Mikulski, M., Balakrishnan, P. R., Storm, X., & Hunicz, J. (2022b). Thermo-kinetic multi-zone modelling of low temperature combustion engines. *Progress in Energy and Combustion Science*, *91*, 100998.

Vasudev, A., Mikulski, M., & Hyvönen, J. (2023). Effects of h2 admixture on RCCI combustio n dual-fuel marine engines: A model-based study-clean propulsion. *IEEES 2023–Proc B*, *2023*, 61–65.

Verhaegh, J., Kupper, F., & Willems, F. (2022). Data-driven air-fuel path control design for robust RCCI engine operation. *Energies*, *15*(6), 2018.

Vlaswinkel, M., & Willems, F. (2023). Cylinder pressure feedback control for ideal thermodynamic cycle tracking: Towards self-learning engines. *IFAC-PapersOnLine*, *56*(2), 8260–8265.

Vlaswinkel, M., & Willems, F. (2024). Data-based in-cylinder pressure model with cyclic variations for combustion control: An RCCI engine application. *Energies*, *17*(8), 1881.

Yao, T., Pei, Y., Zhong, B.-J., Som, S., Lu, T., & Luo, K. H. (2017). A compact skeletal mechanism for n-dodecane with optimized semi-global low-temperature chemistry for diesel engine simulations. *Fuel*, *191*, 339–349. https://doi.org/10.1016/j.fuel.2016.11.083

Zhou, K., Doyle, J. C., & Glover, K. (1996). Robust and Optimal Control. Feher/Prentice Hall Digital and. Prentice Hall. https://books.google.fi/books?id=RPSOQgAACAAJ.